



**TEKNISKA HÖGSKOLAN**  
**HÖGSKOLAN I JÖNKÖPING**

**THERMAL CONDUCTIVITY IN HIGH SILICON  
CAST IRON**

Albano Gómez Saro

EXAM WORK 2013

Materials and Manufacturing - Casting

---

Postadress:  
Box 1026  
551 11 Jönköping

Besöksadress:  
Gjuterigatan 5

Telefon:  
036-10 10 00 (vx)

This exam work has been carried out at the School of Engineering in Jönköping in the subject area: Materials and Manufacturing – Casting. The work is a part of the three-year Bachelor of Science in Engineering programme.

The authors take full responsibility for opinions, conclusions and findings presented.

Examiner: Lennart Elmquist

Supervisor: Lennart Elmquist and Taishi Matsushita

Scope: 15 credits (first cycle)

Date: 2013/06/03

---

Postadress:  
Box 1026  
551 11 Jönköping

Besöksadress:  
Gjuterigatan 5

Telefon:  
036-10 10 00 (vx)

## **Abstract**

In this report the thermal conductivity of five cast irons with different composition is studied. The castings chosen for the project were a standard spheroidal graphite iron (SGI), and two SGI with high silicon contents, and two compacted graphite irons (CGI) with also high silicon contents. Some experiments were done for each studied cast iron as dilatometer, differential scanner calorimeter (DSC) and Laser flash. After the thermal study, a microscope analysis was done in order to obtain the nodularity, the graphite amount and the ferrite and pearlite amount of each cast iron. The goal of the project is investigate the thermal behaviour of casting with high silicon contents and find any kind of relation between the silicon content, the thermal conductivity and the nodularity. The results doesn't report an important influence of the silicon content in the thermal conductivity. Studying the results it is concluded that in applications were high thermal conductivity is required, it is recommended cooling rates corresponding to thickness higher than 50 mm.

## **Keywords**

Compacted Graphite Iron (CGI), Spheroidal Graphite Iron (SGI), high silicon cast iron, thermal conductivity, thermal diffusivity, specific heat, thermal expansion, nodularity.

# Contents

<b>1</b>	<b>Introduction .....</b>	<b>6</b>
1.1	BACKGROUND.....	6
1.2	PURPOSE AND RESEARCH QUESTIONS.....	7
1.3	DELIMITATIONS .....	7
1.4	OUTLINE .....	8
<b>2</b>	<b>Theoretical background .....</b>	<b>9</b>
2.1	PURE IRON .....	9
2.1.1	<i>Allotropes forms of iron.....</i>	<i>10</i>
2.2	FE – C ALLOYS .....	11
2.2.1	<i>Fe-C alloys solidification .....</i>	<i>14</i>
2.2.2	<i>Fe - C alloys phases.....</i>	<i>16</i>
2.2.3	<i>Classification of cast iron.....</i>	<i>18</i>
2.2.4	<i>Metallography .....</i>	<i>24</i>
2.3	HEAT TRANSMISSION .....	26
2.3.1	<i>Heat conduction.....</i>	<i>26</i>
2.3.2	<i>Thermal expansion.....</i>	<i>28</i>
2.3.3	<i>Specific heat capacity .....</i>	<i>28</i>
2.3.4	<i>Thermal diffusivity.....</i>	<i>28</i>
2.3.5	<i>Thermal conductivity.....</i>	<i>28</i>
2.4	TREATMENTS FOR CAST IRON.....	29
2.4.1	<i>Annealing.....</i>	<i>30</i>
2.4.2	<i>Stress relieving .....</i>	<i>31</i>
2.4.3	<i>Normalizing .....</i>	<i>31</i>
2.4.4	<i>Work hardening .....</i>	<i>31</i>
2.4.5	<i>Solid solution strengthening .....</i>	<i>31</i>
2.4.6	<i>Grain-boundary strengthening .....</i>	<i>32</i>
2.4.7	<i>Dispersion strengthening.....</i>	<i>33</i>
<b>3</b>	<b>Method and implementation .....</b>	<b>34</b>
3.1	MATERIALS.....	34
3.2	DILATOMETER .....	36
3.3	ARCHIMEDES’ PRINCIPLE .....	38
3.4	DIFFERENTIAL SCANNING CALORIMETRY (DSC).....	39
3.5	LASER FLASH METHOD .....	41
3.6	SAMPLES PREPARATION AND OPTICAL MICROSCOPE .....	42
<b>4</b>	<b>Findings and analysis.....</b>	<b>45</b>
4.1	THERMAL EXPANSION .....	45
4.2	SPECIFIC HEAT CAPACITY.....	46
4.3	THERMAL DIFFUSIVITY .....	48
4.4	THERMAL CONDUCTIVITY .....	51
4.5	NODULARITY .....	55
4.6	GRAPHITE AND MATRIX AMOUNT.....	58
<b>5</b>	<b>Discussion and conclusions.....</b>	<b>60</b>
5.1	DISCUSSION OF METHOD .....	60
5.1.1	<i>Density.....</i>	<i>60</i>
5.1.2	<i>Thermal expansion.....</i>	<i>60</i>
5.1.3	<i>Specific heat capacity .....</i>	<i>60</i>
5.1.4	<i>Thermal diffusivity.....</i>	<i>61</i>
5.1.5	<i>Graphite amount.....</i>	<i>62</i>

5.2	DISCUSSION OF FINDINGS.....	63
5.2.1	<i>Silicon content and thermal conductivity</i> .....	63
5.2.2	<i>Cooling rate and thermal conductivity</i> .....	63
5.2.3	<i>Nodularity and thermal conductivity</i> .....	63
5.3	CONCLUSIONS.....	64
<b>6</b>	<b>Future work</b> .....	<b>65</b>
<b>7</b>	<b>Acknowledgements</b> .....	<b>66</b>
<b>8</b>	<b>References</b> .....	<b>67</b>
<b>9</b>	<b>Appendices</b> .....	<b>70</b>

## Figures

FIGURE 1. ALLOTROPES OF PURE IRON UPON HEATING AND COOLING [4]	10
FIGURE 2. ATOMIC STRUCTURES OF IRON [4]	11
FIGURE 3. FE-C METASTABLE PHASE DIAGRAM [6]	13
FIGURE 4. HYPOEUTECTOID TRANSFORMATION [7]	15
FIGURE 5. HYPEREUTECTOID TRANSFORMATION [7]	15
FIGURE 6. DENDRITIC GROWING SHAPE [9]	16
FIGURE 7. STRUCTURE OF CEMENTITE [10]	17
FIGURE 8. GRAPHITE STRUCTURE [13]	18
FIGURE 9. GREY CAST IRON OR LAMELLAR GRAPHITE IRON (LGI) [16]	19
FIGURE 10. COMPACTED GRAPHITE IRON (CGI) [17]	20
FIGURE 11. COMPACTED GRAPHITE IN A SCANNING ELECTRON MICROSCOPE [15]	20
FIGURE 12. SPHEROIDAL GRAPHITE IRON (SGI) [17]	22
FIGURE 13. TRANSFORMATION FROM AUSTENITE (FCC) TO MARTENSITE (BCT) [14]	29
FIGURE 14. CASTING PATTERN	34
FIGURE 15. SITUATION OF THE SAMPLES IN THE 50 MM PLATE (UNITS: MILLIMETRES)	35
FIGURE 16. NETZSCH DILATOMETER 402C [19]	36
FIGURE 17. RESULT OF DILATOMETER EXPERIMENT	37
FIGURE 18. KERN ABJ	39
FIGURE 19. NETZSCH DSC 404 C PEGASUS [19]	40
FIGURE 20. NETZSCH LFA 427 [19]	41
FIGURE 21. LASER FLASH METHOD [19]	42
FIGURE 22. SAMPLES MOUNTED IN A BAQUELITE CYLINDER	43
FIGURE 23. STRUERS CITOPRESS [21]	43
FIGURE 24. STRUERS TEGRAMIN [21]	44
FIGURE 25. CP RESULTS FOR THREE THICKNESSES OF CASTING G82B SGI FOR BOTH, HEATING (LEFT) AND COOLING (RIGHT) PROCESSES	46
FIGURE 26. CP RESULTS FOR THREE THICKNESSES OF CASTING G89 SGI FOR BOTH, HEATING (LEFT) AND COOLING (RIGHT) PROCESSES	46
FIGURE 27. CP RESULTS FOR THREE THICKNESSES OF CASTING G89 CGI FOR BOTH, HEATING (LEFT) AND COOLING (RIGHT) PROCESSES	47
FIGURE 28. CP RESULTS FOR THREE DIFFERENT SILICON CONTENT CASTINGS G82B SGI, G88 SGI AND G89 SGI FOR BOTH, HEATING (LEFT) AND COOLING (RIGHT) PROCESSES	47
FIGURE 29. CP RESULTS FOR TWO DIFFERENT SILICON CONTENT CASTINGS G88 CGI AND G89 CGI FOR BOTH, HEATING (LEFT) AND COOLING (RIGHT) PROCESSES	48
FIGURE 30. THERMAL DIFFUSIVITY OF CASTING G82B SGI FOR THE THREE THICKNESSES 15, 50 AND 75 MM OF PLATE	49
FIGURE 31. THERMAL DIFFUSIVITY OF CASTING G89 SGI FOR THE THREE THICKNESSES 15, 50 AND 75 MM OF PLATE	49

FIGURE 32. THERMAL DIFFUSIVITY OF CASTINGS G89 CGI FOR THE THREE THICKNESSES OF PLATE 15, 50 AND 75 MM	50
FIGURE 33. THERMAL DIFFUSIVITY RESULTS FOR THREE DIFFERENT SILICON CONTENT CASTINGS G82B SGI, G88 SGI AND G89 SGI	50
FIGURE 34. THERMAL DIFFUSIVITY RESULTS FOR TWO DIFFERENT SILICON CONTENT CASTINGS G88 CGI AND G89 CGI	51
FIGURE 35. THERMAL CONDUCTIVITY OF CASTING G82B SGI FOR THE THREE THICKNESSES 15, 50 AND 75 MM OF PLATE	52
FIGURE 36. THERMAL CONDUCTIVITY OF CASTING G89 SGI FOR THE THREE THICKNESSES 15, 50 AND 75 MM OF PLATE	52
FIGURE 37. THERMAL CONDUCTIVITY OF CASTING G89 CGI FOR THE THREE THICKNESSES 15, 50 AND 75 MM OF PLATE	53
FIGURE 38. THERMAL CONDUCTIVITY OF 15 MM OF THICKNESS CASTINGS	53
FIGURE 39. THERMAL CONDUCTIVITY OF 75 MM OF THICKNESS CASTINGS	54
FIGURE 40. THERMAL CONDUCTIVITY RESULTS FOR THREE DIFFERENT SILICON CONTENT CASTINGS G82B SGI, G88 SGI AND G89 SGI	54
FIGURE 41. THERMAL CONDUCTIVITY RESULTS FOR TWO DIFFERENT SILICON CONTENT CASTINGS G88 CGI AND G89 CGI	55
FIGURE 42. THERMAL CONDUCTIVITY VERSUS NODULARITY AT ROOM TEMPERATURE	57
FIGURE 43. THICKNESS VERSUS NODULARITY AT ROOM TEMPERATURE	58
FIGURE 44. THERMAL CONDUCTIVITY VERSUS GRAPHITE AMOUNT AT ROOM TEMPERATURE	59
FIGURE 45. G82B SGI 15 MM	77
FIGURE 46. G82B SGI 50 MM	78
FIGURE 47. G82B SGI 75 MM	78
FIGURE 48. G88 SGI 50 MM	78
FIGURE 49. G89 SGI 15 MM	79
FIGURE 50. G89 SGI 50 MM	79
FIGURE 51. G89 SGI 75 MM	79
FIGURE 52. G88 CGI 50 MM	80
FIGURE 53. G89 CGI 15 MM	80
FIGURE 54. G89 CGI 50 MM	80
FIGURE 55. G89 CGI 75 MM	81

## Tables

TABLE 1. PROPERTIES OF PURE IRON [2]	9
TABLE 2. MAIN COMPONENTS ANALYSIS OF EACH CASTING	34
TABLE 3. THERMAL EXPANSION VALUES, $\Delta E / 10^{-6} \cdot K^{-1}$	45
TABLE 4. NODULARITY (%) OF ALL THE STUDIED CASTINGS AND THICKNESSES	56
TABLE 5. GRAPHITE AND FERRITE/PERLITE AMOUNTS	58
TABLE 6. COMPLETE COMPONENTS ANALYSIS OF EACH CASTING	70
TABLE 7. THERMAL CONDUCTIVITY VALUES OF CASTING G82B SGI 15 MM	74
TABLE 8. THERMAL CONDUCTIVITY VALUES OF CASTING G82B SGI 50 MM	75
TABLE 9. THERMAL CONDUCTIVITY VALUES OF CASTING G82B SGI 75 MM	75
TABLE 10. THERMAL CONDUCTIVITY VALUES OF CASTING G89 SGI 15 MM	75
TABLE 11. THERMAL CONDUCTIVITY VALUES OF CASTING G89 SGI 50 MM	75
TABLE 12. THERMAL CONDUCTIVITY VALUES OF CASTING G89 SGI 75 MM	76
TABLE 13. THERMAL CONDUCTIVITY VALUES OF CASTING G88 SGI 50 MM	76
TABLE 14. THERMAL CONDUCTIVITY VALUES OF CASTING G89 CGI 15 MM	76
TABLE 15. THERMAL CONDUCTIVITY VALUES OF CASTING G89 CGI 50 MM	76
TABLE 16. THERMAL CONDUCTIVITY VALUES OF CASTING G89 CGI 75 MM	77
TABLE 17. THERMAL CONDUCTIVITY VALUES OF CASTING G88 CGI 50 MM	77

# **1 Introduction**

This report describes the final work done as part of the author's education of Industrial Engineering, conducted on the Cantabria's University. It has been carried out in the workshop and laboratory of Jönköping's University (Sweden) where the author studied one year (2012-2013) as exchange student.

This project is part of larger projects which goal is study if compact graphite irons (CGI) and spheroidal graphite irons (SGI) would be suitable for different purposes as the manufacture of the cylinder heads of trucks with diesel engines.

This report is focus on the thermal properties of the castings and attempts to gain some relationship between the cooling rate, the nodularity or the amount of silicon in a casting and the thermal properties as specific heat capacity, thermal expansion, thermal diffusivity or thermal conductivity of these castings.

## **1.1 Background**

Due to the increasing number of materials being used in high temperature applications, knowledge of their thermophysical properties, especially thermal conductivity, is of paramount importance. This report investigates the thermal properties of the casting, with the aim of finding a material more suitable than current.

For example currently, cylinder heads of diesel truck engines are manufactured in lamellar graphite iron (LGI) with pearlite matrix because it is easy to machine due to the graphite instead being a brittle material. The features that should have the material are enough hardness and strength to withstand the high pressures generated inside the engine and high thermal conductivity to evacuate the maximum amount of heat from inside the chamber avoiding overheat problems in the engine.

## **1.2 Purpose and research questions**

In this project the thermal conductivity depending of the temperature of five different castings had been studied in order to determine if they would be suitable for the manufacture of some products like the cylinder heads of the diesel truck engine. The materials studied were CGI and SGI with high content of silicon and ferrite matrix, easier and therefore cheaper to manufacture than pearlite matrix castings, subsequently treated with heat treatment to increase its hardness. The highest temperature inside the piston chamber in normal conditions is lower than 300 °C as explained in the paper [1], in this project the samples were heated to 500 °C in order to take advantage of the results for others future projects. Also the microstructure of each material is analysed with a microscope and software was applied in order to get the nodularity. The aim of this project is answer these questions:

- Is there any relationship between the silicon content and the thermal conductivity?
- Is there any relationship between the cooling rate and the thermal conductivity in high silicon castings?
- Is there any relationship between the nodularity and the thermal conductivity in high silicon castings?

## **1.3 Delimitations**

- The materials studied on this project are CGI and SGI. LGI was discarded because is more common and known than the others.
- The nodularity and thermal properties of the cast irons are studied, other mechanical properties as hardness, strain, stress or elasticity of the materials chosen is not study in this project.
- Any kind of mathematical regression analysis is not studied on this report.

## **1.4 Outline**

In the chapter two “Theoretical background” is summarized the most general fields of cast iron and thermal properties.

The chapter three “Method and implementation” contains an explanation and description of the methods, experiments and equipment chosen in this project and what they involve.

In the chapter four “Findings and analysis” are presented all the objective findings and results of the work, and a subjective analysis of them.

The chapter five “Discussion and conclusions” is divided in three parts. In the first part “Discussion of method” it is explained the choice of the methods and how well the results are obtained in regard to the purpose and the research questions of the project. In the second part “Discussion of findings” the analysed findings are evaluated with regard to the purpose and the research questions of the project. The third part “Conclusions” summaries the main points obtained.

## 2 Theoretical background

### 2.1 Pure Iron

Iron is a chemical element with the symbol Fe (from Latin “ferrum”), it is a metal with atomic number 26. It is present in the outer and inner core of the Earth, being the fourth most common element in the Earth's crust. Most important pure iron properties at room temperature are exposed on Table 1.

Table 1. Properties of pure iron [2]

Property	Value
Standard atomic weight	55.845 g·mol <sup>-1</sup>
Density (near room temperature)	7.874 g·cm <sup>-3</sup>
Liquid density at melting point	6.98 g·cm <sup>-3</sup>
Melting point	1811 K, 1538 °C, 2800 °F
Boiling point	3134 K, 2862 °C, 5182 °F
Heat of fusion	13.81 kJ·mol <sup>-1</sup>
Heat of vaporization	340 kJ·mol <sup>-1</sup>
Molar heat capacity	25.10 J·mol <sup>-1</sup> ·K <sup>-1</sup>
Atomic radius	126 pm
Electrical resistivity at 20 °C	96.1 nΩ·m
Thermal conductivity	80.4 W·m <sup>-1</sup> ·K <sup>-1</sup>
Thermal expansion at 25 °C	11.8 μm·m <sup>-1</sup> ·K <sup>-1</sup>
Young's modulus	211 GPa
Vickers hardness	608 MPa
Brinell hardness	490 MPa

Iron exists naturally in iron ore (or ironstone). In this form, iron is even softer than aluminium. Since iron has a strong affinity for oxygen, iron ore is an oxide of iron, it also contains varying quantities of other elements such as silicon, sulphur, manganese and phosphorus. Smelting is the process by which iron is extracted from iron ore.

Bronze and copper alloys have been used since ancient times in implements and weapons due to their low melting temperatures. The production of iron by humans began probably sometime after 2000 before Christ (BC) in somewhere of Asia. Since then, for over three thousand years, until replaced by steel after 1870 after Christ (AC), iron formed the material basis of human civilization in Europe, Asia and Africa [3].

### 2.1.1 Allotropes forms of iron

Pure iron exhibits polymorphism, it exists in more than one space lattice in the solid state. Polymorphism refers to the ability of a chemical substance to exist in more than one form or crystal structure. When polymorphism occurs in elemental solids, it is called allotropy and the different forms of the solid are called allotropes. The changes of state between solid, liquid and gas in themselves are not considered allotropy. The Figure 1 shows all the pure iron allotropies and considers the temperatures of formation for heating and cooling process equals, this is an approximation and in reality these temperatures are not exactly equal.

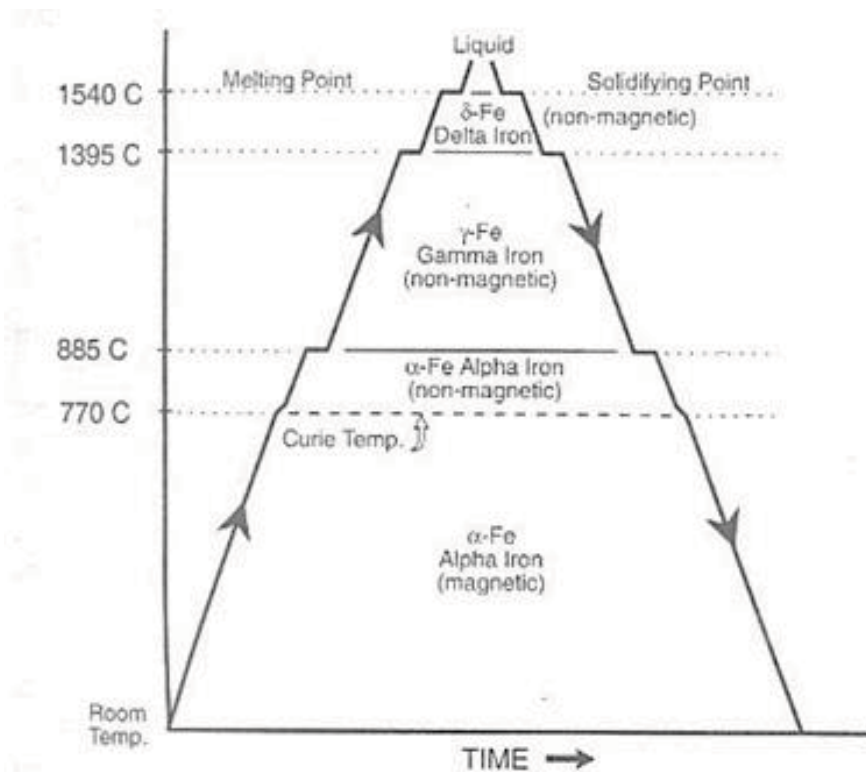


Figure 1. Allotropes of pure iron upon heating and cooling [4]

At atmospheric pressure there are three allotropic forms of iron: alpha iron ( $\alpha$ -Fe), gamma iron ( $\gamma$ -Fe) and delta iron ( $\delta$ -Fe). As going down the temperature of the molten iron, it will transform in all this allotropes:

- Delta iron ( $\delta$ -Fe): the molten iron crystallizes at 1538 °C into its  $\delta$  allotrope which has a body centered cubic (BCC) crystal structure shown in the Figure 2.
- Gamma iron ( $\gamma$ -Fe): as the iron cools further to 1394 °C its crystal structure changes to a face centered cubic (FCC) crystal structure shown in the Figure 2.

- Alpha iron ( $\alpha$ -Fe): at 912 °C the crystal structure again becomes BCC crystal structure as  $\alpha$ -iron is formed. The iron is at this temperature is non-magnetic. At 770 °C called Curie temperature, the iron is a fairly soft metal. There is no change in crystalline structure but there is a change in the magnetic properties and it becomes ferromagnetic. This is the stable form of iron at room temperature.

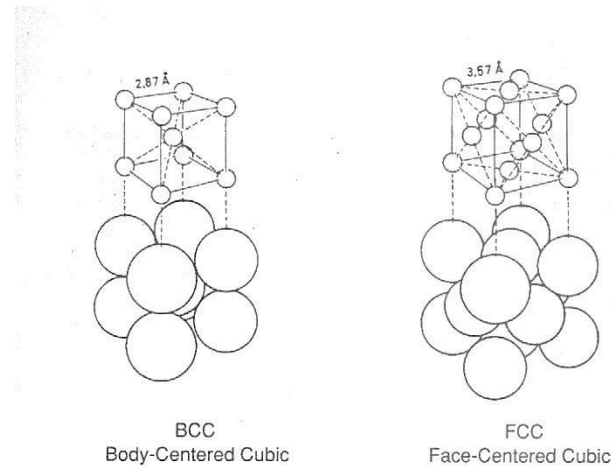


Figure 2. Atomic structures of iron [4]

The allotropic transformations illustrated are reversible, such that the transformations can occur upon slow heating or slow cooling. It is this powerful flexibility of iron that provides the opportunity to heat treated irons and steels to many metallurgical conditions and associated mechanical and physical properties.

## 2.2 Fe – C alloys

Fe-C and other metals alloys are the most common metals in industrial use. This is mainly due to two characteristics, first it great range of properties and second the abundance of iron in the Earth.

Cast iron and steels are alloys consisting mainly of iron, carbon and other substances with lower proportion like silicon, manganese, nickel, magnesium, sulphur or phosphorus. These are the properties that offer each of the elements that most common appear specifically in cast iron.

- Carbon: reduces the mechanical properties of the castings and its content is set between 2.5 and 4 wt%. Resistant castings have low carbon, on the other hand, it reduces the tendency to hardening and improves moulding accuracy.

- Silicon: graphitic element fundamental for grey cast irons. Its content should be taken according to the section of the piece to melt. Normal levels of silicon in a melting vary between 1 to 3.8 wt%. Increasing silicon content favour ferritic structure and increase the hardness of the ferrite.
- Sulphur: this element is adding to the casting during melting so that it is not possible to avoid its presence in the composition, its content should be as reduced as possible. Sulphur and iron forms iron sulphide (FeS), solid to 988 °C, it is segregated FeS in the grain boundaries increasing casting hardness and brittleness and is harmful because it hinders graphitization. Manganese addition forms manganese sulphide (MnS), solid to 1620 °C, this temperature is much higher when the manganese content is stronger. These sulphide inclusions are found in grey hexagonal inclusions, isolated of the structure and without inconvenience to the mechanical characteristics. Sulphur also causes cooling effects and worsens the properties of cast iron (particularly low fluency). Also the sulphur plays an important role in the nucleation of graphite. The sulphur and manganese content are related by the following equation:

$$Mn \geq 1.7\% S + 0.3 \quad (1)$$

- Manganese: it has the essential function of fixing the sulphur by the above equation. Apart from this manganese eventually stabilizes the pearlite and cementite. Manganese has an effect opposite to that of silicon, it prevents the graphitization.
- Phosphorus: it has almost no effect on the graphitization, however is an impurity in the iron useful as it improves fluency. Which gives fluidity to the iron phosphorus is due to the formation of a eutectic solidification at low temperature (950 °C), commonly called steadite. It is a ternary eutectic formed by austenite and cementite and iron phosphide (Fe<sub>3</sub>P) to 2 wt% C and 6.9% S, or eutectic pseudobinary, formed by austenite, graphite and Fe<sub>3</sub>P. Steadite meets virtually all the phosphorus composition and favours direct segregations of carbures. Appears in cells and it could form a continuous network of steadite with sufficiently high phosphorus content (P > 0.3 wt%). In general, the steadite is formed when the phosphorus content is greater than 0.15 wt%. High levels of this element can promote shrinkage porosity while low levels of phosphorus increase the cast ability of the metal within the mould. The phosphide eutectic increased total hardness and wear resistance of the cast iron. The level of phosphorus in the Grey iron should be approximately in the range of 0.02 to 0.10 wt% P.

The metal is very versatile and it is possible to obtain a wide range of mechanical and physical properties by adjusting alloying content or by heat treatments. The nomenclature of cast irons and steels is confused due to there are so many ways to describe the same material as countries and institutions related to their manufacture and use. In America, they use the ASTM (American Society for Testing and Materials) and AISI (American Iron and Steel Institute) [5].

To study the different phases of the alloys there are two types of diagrams that show the evolution of the alloy solidification from the liquid phase at high temperatures to room temperature. Stable phase diagrams show the process according to the percentage of the total weight of the alloy containing graphite and metastable phase diagrams, based on the total weight percentage of cementite. The name is because the cementite is very unstable phase.

In order to develop an understanding of cast iron the binary Fe-C metastable phase diagram showed in the Figure 3 is commonly studied, it describes the iron - carbon system of alloys containing less than 6.67 wt% C, discloses the phase's compositions and their transformations occurring with the alloys during their cooling or heating. Carbon content 6.67 wt% C corresponds to the fixed composition of the iron carbide  $Fe_3C$ .

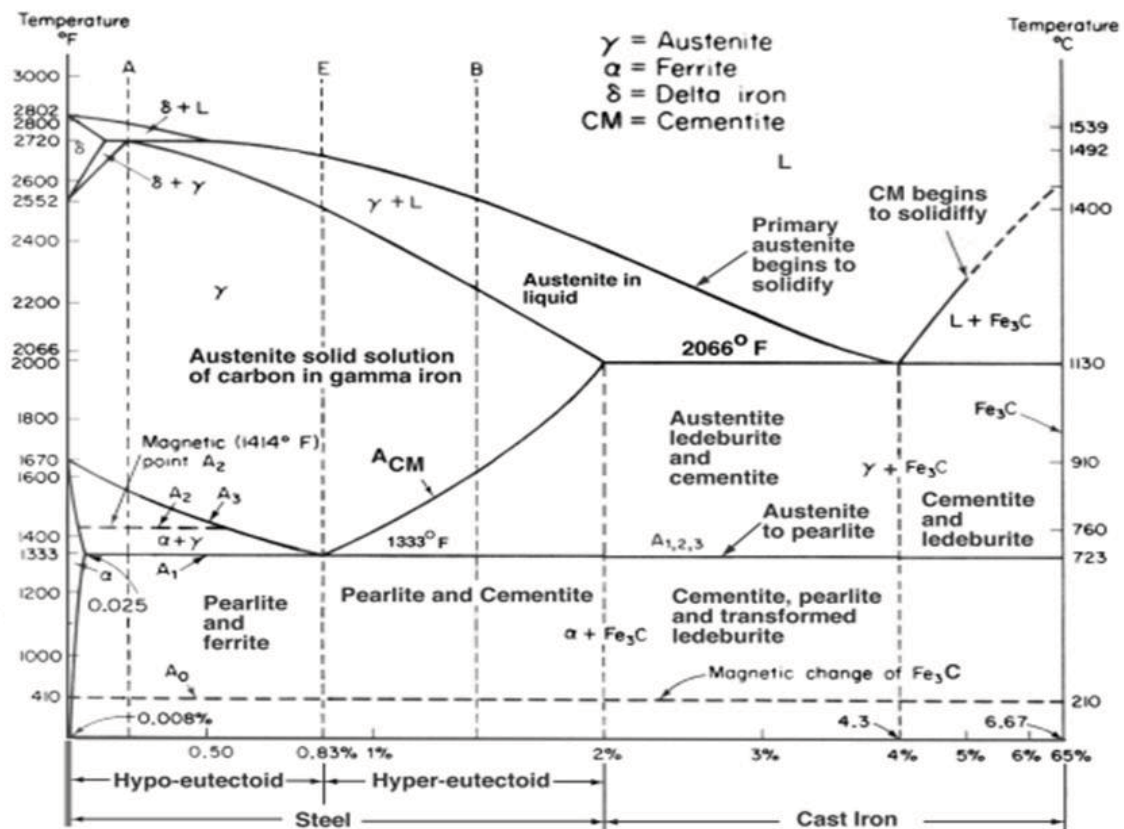


Figure 3. Fe-C metastable phase diagram [6]

Most commercial grey irons are produced with carbon levels from 2.5 to 4 wt% C. normal levels of silicon varies from 1 to 3.8 wt% Si and it also can contain more element as phosphorus. Using the carbon equivalent (CE) concept, it is possible to describe the effect of carbon, silicon and phosphorus in binary Fe – C metastable phase diagram. The idea is to convert the percentage of alloying elements other than carbon to the equivalent carbon percentage. The CE can be calculated with the equation:

$$CE(\%) = \%C + \frac{\%Si + \%P}{3} \quad (2)$$

### 2.2.1 Fe-C alloys solidification

In the Fe – C diagram there are three critical points where invariant reactions are produced. That means that it is in thermal equilibrium, so the number of degrees of freedom at the Gibbs' phase rule is equal zero.

$$F = C - P + 2 \quad (3)$$

Where:

F: number of degrees of freedom

C: number of components

P: number of phases in thermodynamic equilibrium (solid, liquid and gas)

In the Fe-C diagram three invariants reaction are presented and the solidification process of the melt change at both sides of these points.

- Peritectic reaction (composition 0.09 wt% C at 1495 °C)

A liquid and solid phase, in this case delta iron, react to yield a single solid phase, austenite. The process is slow due to the diffusion barrier produced, so when a peritectic composition solidifies, it doesn't show the lamellar structure that is found with eutectic solidification. This point is outside the cast irons carbon content range, so it is not deeply studied in this project.

- Eutectoid reaction (composition 0.83 wt% C at 723 °C)

The austenite phase undergoes a eutectoid transformation to produce ferrite and cementite. The microstructure after the transformation is formed by two phases, a matrix that can vary with the cooling speed and other phase of graphite or cementite. When alloy of eutectoid composition is cooled very slowly it forms a complete ferrite matrix. If the alloy is cooled slowly it forms a ferritic-pearlitic matrix. When alloy of eutectoid composition is cooled fast, it forms a pearlitic matrix. If the alloy is cooled very fast, bainite or martensite matrix could be obtained.

If the CE is below 0.83 wt% C the composition is said to be hypoeutectoid. It contains proeutectoid ferrite, formed above the eutectoid temperature plus the eutectoid perlite that contain eutectoid ferrite and cementite. The process is represented in the Figure 4.

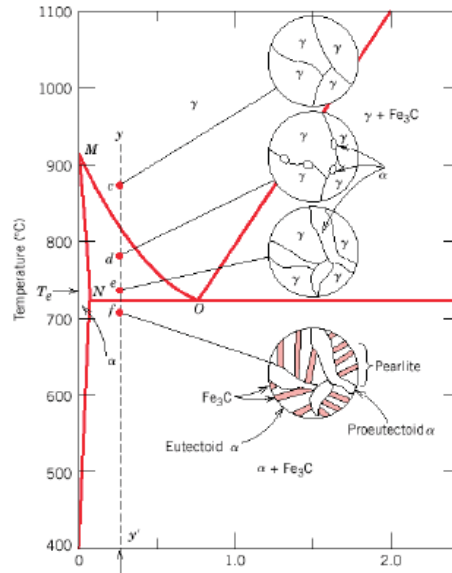


Figure 4. Hypoeutectoid transformation [7]

If the CE is above than 0.83 wt% C the composition is said to be hypereutectoid. It contains proeutectoid cementite (formed above the eutectoid temperature) plus pearlite that contain eutectoid ferrite and cementite. The process is represented in Figure 5.

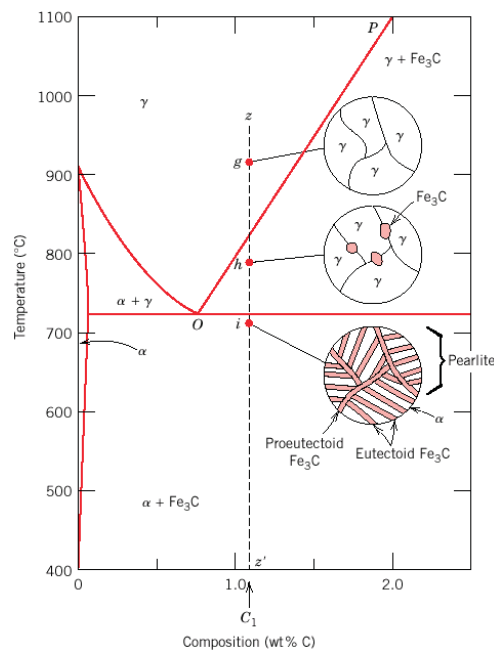


Figure 5. Hypereutectoid transformation [7]

- Eutectic reaction (composition 4.3 wt% C at 1130 °C)

The liquid phase undergoes a eutectic transformation to produce austenite and carbure (in graphite or cementite form). If the CE is below 4.3 wt% C the composition is said to be hypoeutectic which means that primary austenite will form prior to the eutectic reaction. This primary austenite is known as dendrite due to the dendritic growing shape, from a to d, shown in Figure 6. This is the typical solidification process for grey cast iron. An extent review of solidification process historical study of grey cast iron is written by D. M. Stefanescu [8]. If the CE is above than 4.3 wt% C the composition is said to be hypereutectic and a primary phase of graphite or cementite will precipitate prior to the eutectic reaction.

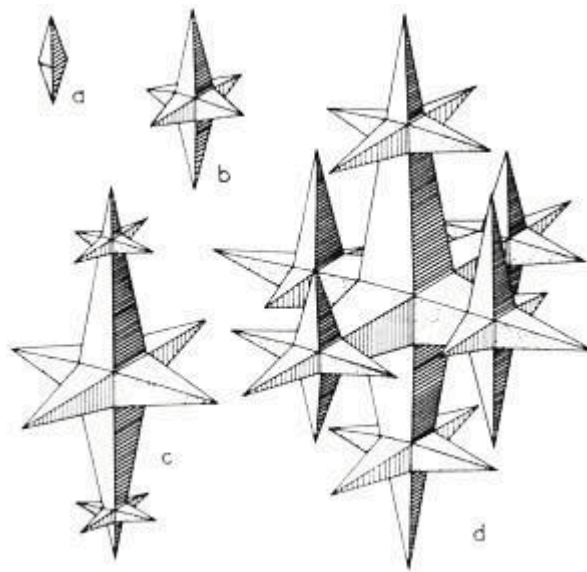


Figure 6. Dendritic growing shape [9]

The microstructure below the eutectic transformation can vary with the cooling rate. If an alloy of eutectic composition is cooled slowly it forms austenite matrix with graphite and ferrite growing in graphite borders. If the alloy is cooled fast it forms an austenite matrix with graphite.

### **2.2.2 Fe - C alloys phases**

These are the phases involved in iron and carbon alloys, each one has its own properties:

- Ferrite: solid solution of carbon between atoms of  $\alpha$  - iron with body centered cubic (BCC) crystal structure. The maximum solubility of carbon is 0.02 wt% C at 727 °C and the minimum is  $5 \cdot 10^{-5}$  wt% C at 20 °C. Ferrite is soft and ductile, it has strength of 280 N/mm<sup>2</sup>, a hardness of approximately 80 Brinell and it is ferromagnetic up to 768 °C.
- Austenite: solid solution of carbon between atoms of  $\gamma$ -iron with face centered cubic (FCC) crystal structure. The maximum solubility of carbon is 2.1 wt% at 1146 °C which decreases to 0.77 wt% at 727 °C. The solubility in austenite is larger compared to ferrite. It is soft, ductile, malleable, tough and non-magnetic.
- Cementite (Fe<sub>3</sub>C): interstitial intermetallic compound having fixed carbon content of 6.67 wt% C. It has a complex orthorhombic structure, with 12 Fe atoms and 4 C atoms per unit cell. High hardness, brittle, very low tensile strength and high compressive strength. It is the hardest phase that appears on the phase diagram. Its structure is represented in Figure 7.

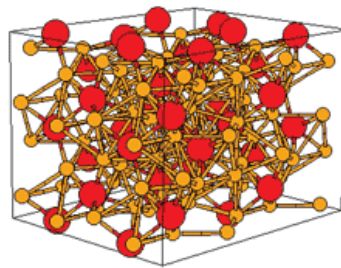


Figure 7. Structure of cementite [10]

- Pearlite: it is eutectoid mixture of ferrite (86.5%) and cementite (13.5%) containing 0.8 wt% C and is formed at 727 °C. In a two dimensions figure it present a lamellar appearance but in three dimensions both components ferrite and cementite are interconnected in regions called colonies. It is harder than ferrite.
- Ledeburite: it is eutectic mixture of austenite and cementite. It contains 4.3 wt% C and is formed below 1146 °C.
- Bainite: is an acicular (needle shaped crystals) microstructure (not a phase) that forms in steels at temperatures from approximately 250-550 °C, depending on alloy content. It is an intermediate of pearlite and martensite in terms of hardness. For this reason, the bainitic microstructure becomes useful in that no additional heat treatments are required after initial cooling to achieve a hardness value between that of pearlitic and martensitic steels.
- Martensite: the second hardest form of steel crystalline structure after Cementite, it is formed by rapid cooling (quenching) of austenite which traps carbon atoms that do not have time to diffuse out of the crystal structure.

- Steadite: the eutectic of ferrite and iron phosphide ( $\text{Fe}_3\text{P}$ ), composition of the eutectic is 10.2% phosphorus and 89.8% iron, it melts at 1049 °C. It is hard structural.
- Graphite: it is the most stable form of carbon under standard conditions. It is an electrical conductor, a semimetal. It is, consequently, useful in such applications as arc lamp electrodes. Its structure is represented in Figure 8. As explained below in chapter 2.2.4 depending on the graphite shape the cast iron can be classified in three types: lamellar, compact and spheroidal graphite iron. In lamellar graphite iron the dominant growth direction of graphite occurs along an axis and the thermal conductivity is high. In compact graphite iron there is not any preferred growth direction being a complex process deeply study in other projects as [11]. The thermal conductivity is between LGI and SGI. In spheroidal graphite iron the graphite growth occurs in radial manner along the c axis and the thermal conductivity is low. An extent study of the thermal conductivity of each kind of casting can be found in the paper [12].

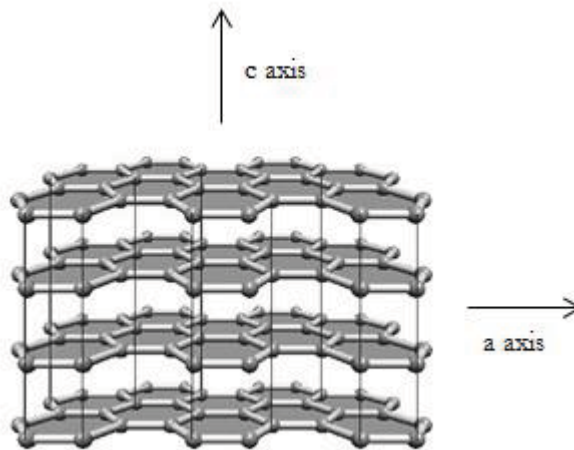


Figure 8. Graphite structure [13]

### 2.2.3 Classification of cast iron

In the all history the classification of the cast iron is confusing due to the development of the microscope that allows the study of the microstructure of the material. In this report the cast iron is divided in grey cast iron, compacted graphite iron (CGI) and spheroidal graphite iron (SGI). The information summarized in this section is taken from the references [14] and [15].

- Grey cast iron

It is a type of cast iron that has a microstructure formed by a matrix with graphite inclusions. The name came for the colour of the fracture that it forms, which is

due to the presence of graphite. Grey iron is a common engineering alloy because of its relatively low cost and good machinability, which results from the graphite lubricating the cut and breaking up the chips

The graphite takes on the shape of a three dimensional flake. In two dimensions, as a polished surface will appear under a microscope, the graphite flakes appear as fine lines as shown in Figure 9 and because that grey cast iron is known also lamellar graphite iron (LGI).



Figure 9. Grey cast iron or lamellar graphite iron (LGI) [16]

A typical chemical composition to obtain a graphitic microstructure is 2.5 to 4.0 wt% C and 1 to 3 wt% silicon. Silicon is important to making grey iron as opposed to white cast iron, because silicon is a graphite stabilizing element in cast iron, which means it helps the alloy produce graphite instead of iron carbides.

Grey cast iron has reasonable tensile strength of 108-340 MPa associated with a very high compressive strength, making it very suitable for applications requiring rigidity and a low melting temperature (1140-1200 °C). The tips of the flakes act as notches, therefore, it is brittle. The presence of graphite flakes makes the grey iron easily machinable as they tend to crack easily across the graphite flakes. Grey iron also has very good damping capacity because graphite absorbs the energy and hence it is mostly used as the base for machine tool mountings. It has good galling and wear resistance because the graphite flakes self-lubricate. It also experiences less solidification shrinkage than other cast irons that do not form a graphite microstructure. The silicon promotes good corrosion resistance and increase fluidity when casting. Grey iron is generally considered easy to weld. Compared to the more modern iron alloys, grey iron has a low tensile strength and ductility; therefore, its impact and shock resistance is almost non-existent.

Due to the high grey cast iron thermal conductivity and specific heat capacity is employed in applications as cylinder blocks, pump housings, valve bodies, electrical boxes, cast iron cookware and disc brake rotors.

- Compacted graphite iron (CGI)

It is also known as vermicular graphite iron. The graphite particles have a compact or wormlike shape as shows Figure 10 and the three-dimensional structure becomes apparent in a scanning electron microscope after the metallic matrix is removed by etching as shows Figure 11. CGI is a transitional form between LGI and SGI, which occurs when the material is deliberately given insufficient treatment or treatment is interrupted in the process of forming SGI, in fact, it was initially considered a degraded form of cast iron but due to its interesting properties finally, in 1955, the intentional production of CGI was first achieved by Estes and Scheidewind. It falls between LGI and SGI, in terms of microstructure formation and physical properties, which are heavily dependent on the ferrite-to-pearlite ratio in the basic structure.

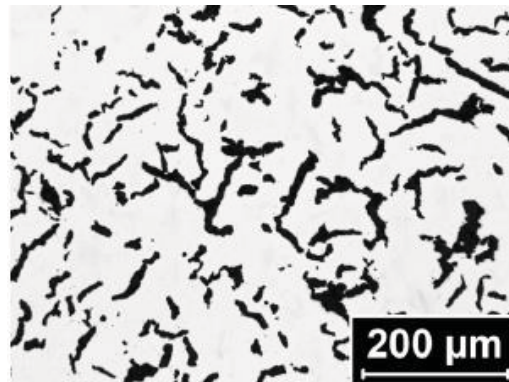


Figure 10. Compacted graphite iron (CGI) [17]

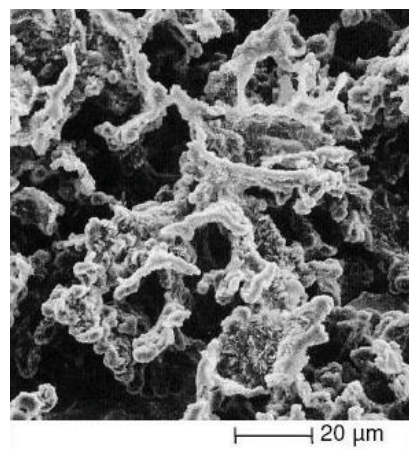


Figure 11. Compacted graphite in a scanning electron microscope [15]

Compared to LGI, CGI provides the following advantages in terms of properties: higher strength and elongation at fracture, higher fracture toughness and its properties are less dependent on the wall thickness than in LGI.

Compared to SGI, CGI offers the following advantages: lower coefficient of thermal expansion but higher heat conductivity, lower modulus of elasticity, lower thermally induced internal stress level, better damping capacity and better pouring properties, like shrinkage, mould filling characteristics or fluidity.

However, despite being an alloy known for decades and its interesting properties, CGI exploitation has never taken the leap necessary to become a reference material in the market. The low accuracy of established methods of process control, able to ensure consistency in structure and physical properties in the manufactured parts, has caused customers to choose other grades of iron. The problem is associated with the particular variations of the production processes for the manufacture of CGI. Usually CGI is made like ductile iron, some magnesium or caesium is added to the melt as nodulizer and also any graphite degenerate promoter can be added, as Ti or S. The vermicular rate depends on the balance between the different graphite shape modifiers (Mg, Ce, S, Ti, Al, O, etc.), the cooling rate and the ability to form graphitic core or nucleation ability. The variations in the yield of the additions, with the narrow ranges allowed for the combination of those elements, and the uncertainty of the chemical composition analysis devices, causes a customer rejection because the material does not meet its specifications.

CGI is especially suitable for components which are exposed to both thermal and mechanical stresses. Examples include cylinder heads, exhaust manifolds and brake parts, but vermicular graphite is also used for the manufacture of transmission domes for cars and engine units for trucks and cars.

- Spheroidal graphite iron (SGI)

It is also known as ductile cast iron, ductile iron or nodular cast iron is a type of cast iron invented in 1943 by Keith Millis. While most varieties of cast iron are brittle, ductile iron is much more flexible and elastic due to its nodular graphite inclusions.

SGI is not a single material but is part of a group of materials which can be produced to have a wide range of properties through control of the microstructure. The common defining characteristic of this group of materials is the morphological structure of the graphite. In ductile irons, the graphite is in the form of spherical nodules shown in Figure 12 rather than flakes (as in grey cast iron), thus inhibiting the creation of cracks and providing the enhanced ductility that gives the alloy its name.

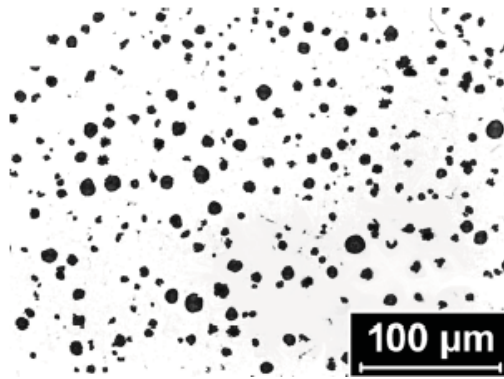


Figure 12. Spheroidal graphite iron (SGI) [17]

Austempered Ductile Iron (ADI) was invented in the 1950s but was commercialized and achieved success only some years later. In ADI, the metallurgical structure is manipulated through a sophisticated heat treating process. The "aus" portion of the name refers to austenite.

A typical chemical analysis of this material: iron, carbon (3.3-3.4 wt%), silicon (2.2-2.8 wt%), manganese (0.1-0.5 wt%), magnesium (0.03-0.05 wt%), phosphorus ( $5 \cdot 10^{-3}$ -0.04 wt%) and sulphur ( $5 \cdot 10^{-3}$ -0.02 wt%). Other elements such as copper or tin may be added to increase tensile and yield strength while simultaneously reducing elongation. Improved corrosion resistance can be achieved by replacing 15% to 30 wt% of the iron in the alloy with varying amounts of nickel, copper or chromium.

Much of the annual production of SGI is in the form of ductile iron pipe, used for water and sewer lines. It competes with polymeric materials such as PVC, HDPE, LDPE and polypropylene which are all much lighter than steel or ductile iron but which, being flexible, require more careful installation and protection from physical damage.

The possible applications of SGI are very wide. The properties are such as to extend the field of usefulness of cast iron and enable it, for some purpose, to replace steel casting, malleable cast iron, and non-ferrous alloys. But SGI is not recommended as a replacement for all castings at present made in grey cast iron, sometimes the inherent properties of the grey cast iron are adequate for the purpose of existing designs. The use SGI is suggested where improved properties are dictate a replacement of other material or where the use of SGI will permit an improvement in the design. Some popular uses of SGI for various engineering application are for support bracket for agricultural tractor, tractor life arm, check beam for lifting track, mine cage guide brackets gear wheel and pinion blanks and brake drum, machines worm steel, flywheel, thrust bearing, frame for high speed diesel engine, four throw crankshaft, fully machined piston for large marine diesel engine, bevel wheel, hydraulic clutch on diesel engine for heavy vehicle, fittings overhead electric transmission lines, boiler mountings, etc.

- White cast iron

It is the iron that displays white fractured surface due to the presence of cementite. With a lower silicon content and faster cooling, the carbon in white cast iron precipitates out of the melt as the metastable phase cementite,  $\text{Fe}_3\text{C}$ , rather than graphite. The cementite which precipitates from the melt forms as relatively large particles, usually in a eutectic mixture where the other phase is austenite (which on cooling might transform to martensite). These eutectic carbides are much too large to provide precipitation hardening (as in some steels, where cementite precipitates might inhibit plastic deformation by impeding the movement of dislocations through the ferrite matrix). Rather, they increase the bulk hardness of the cast iron simply by virtue of their own very high hardness and their substantial volume fraction, such that the bulk hardness can be approximated by a rule of mixtures. In any case, they offer hardness at the expense of toughness. Since carbide makes up a large fraction of the material, white cast iron could reasonably be classified as a cermet. White iron is too brittle for use in many structural components, but with good hardness and abrasion resistance and relatively low cost, it finds use in such applications as the wear surfaces (impeller and volute) of slurry pumps, shell liners and lifter bars in ball mills and autogenous grinding mills, balls and rings in coal pulverisers and the teeth of a backhoe's digging bucket (although cast medium-carbon martensitic steel is more common for this application).

It is difficult to cool thick castings fast enough to solidify the melt as white cast iron all the way through. However, rapid cooling can be used to solidify a shell of white cast iron, after which the remainder cools more slowly to form a core of grey cast iron. The resulting casting, called a chilled casting, has the benefits of a hard surface and a somewhat tougher interior.

High-chromium white iron alloys allow massive castings (for example, a 10 tonne impeller) to be sand cast due to a high cooling rate is not required, as well as providing impressive abrasion resistance.

## **2.2.4 Metallography**

Metals, except in a few instances, are crystalline in nature and, except for single crystals, they contain internal boundaries known as grain boundaries. When a new grain is nucleated during processing (as in solidification or annealing after cold working), the atoms within each growing grain are lined up in a specific pattern that depends upon the crystal structure of the metal or alloy. With growth, each grain will eventually impinge on others and form an interface where the atomic orientations are different.

As early as the year 1900, it was well known that most mechanical properties were improved as the size of the grains decreased. A few notable exceptions exist where a coarse grain structure is desired. Alloy composition and processing must be controlled to achieve the desired grain size. Metallography examines polished cross sections of specimens from appropriate locations to determine the grain size. Grain size measurement is complicated due to some factors as:

- The three-dimensional size of the grains is not constant and the sectioning plane will cut through the grains at random. Thus, on a cross-section we will observe a range of sizes, none larger than the cross section of the largest grain sampled. Grain shape also varies, particularly as a function of grain size.
- Grain size measurement is also complicated by the different types of grains that can be present in metals, although their fundamental shapes are the same.
- In heat-treated steels, it is recognized that the grain size of the product of the heat treatment, usually martensite, is not measured or cannot be measured.
- Another complicating factor is the different measures of grain size.

There has been defined various standards, the most commons are ASTM (American Section of the International Association for Testing Materials) and ISO (International Standard Organization), but there are more methods like VDG. The ASTM standard describes various methods for measuring grain size [18]:

- Comparison procedure: involves comparing grain structure with a series of graduated images.
- Planimetric procedure: involves counting the number of grains within a given area.
- Intersection procedure: involves counting the grains intercepted by a test line or the number of intersections of the line with grain boundaries.

The most used is the planimetric procedure explained below. There are two different versions depending of the units system of the country:

Countries that use the imperial units system, like United States, Canada and the United Kingdom express grain sizes in terms of a simple exponential equation:

$$n = 2^{N-1} \quad (4)$$

Where:

n: number of grains per square inch at 100x magnification

N: ASTM grain size number

Countries like Sweden or Spain that used the metric system, at that time developed an alternate equation that produces nearly identical grain size numbers:

$$m = 8 \cdot 2^G \quad (5)$$

Where:

m: number of grains per mm<sup>2</sup> at 1x magnification

G: metric grain size number

G is slightly greater than N. and they are related by this equation:

$$N - G = 0.0458 \quad (6)$$

The ISO method stipulates that at least 80% of the graphite particles viewed on a two dimensional polished surface should have a compacted shape, and less than 20% should have a more round shape, to be classified as CGI. No lamellar shaped graphite particles are permitted. To simplify the determination of which particles have a compacted shape, the standard uses a roundness shape factor (RSF) defined as:

$$RSF = \frac{A}{A_m} = \frac{4 \cdot A}{\pi \cdot l_m^2} \quad (7)$$

Where:

A: area of the graphite particle seen on a polished surface

l<sub>m</sub>: the maximum length of the graphite particle

A<sub>m</sub>: the area of the circle with the diameter l<sub>m</sub>

The RSF is subsequently used to divide the graphite particles into three different groups. RSF values between 0.625 and 1 are defined as nodules, between 0.525 and 0.625 are defined as intermediate and values below 0.525 are defined as compacted. Particles having l<sub>m</sub> smaller than 10 μm are excluded from the calculations. The nodularity is calculated using these values, as follows:

$$\text{Nodularity}(\%) = \frac{\Sigma A_{\text{nodule}} + 0.5 \Sigma A_{\text{intermediate}}}{\Sigma A_{\text{all-particles}}} \cdot 100 \quad (8)$$

Where:

$A_{\text{nodule}}$ : area of the graphite particles classified as nodules

$A_{\text{intermediate}}$ : area of the particles classified as intermediate shaped

$A_{\text{all-particles}}$ : area of all particles exceeding 10  $\mu\text{m}$

The nodularity ranges a negative number for a lamellar graphite iron, in the case of compact graphite iron, the nodularity is in the interval 0-20% and for spheroidal graphite iron it is in the interval 80-100%. The nodularity interval between 20-80% represents a mixture of CGI and SGI.

## 2.3 Heat transmission

To make the best possible use of heat, it is important to know how it is transferred from one point to another and how its movement can be stopped. Heat always flows from a warmer temperature to a colder temperature. The transfer rate of heat flow depends upon the temperature difference. The transmission of heat from one location to another depends a great deal on the material of the flow path. Heat will flow effectively through solids, liquids and gases. The transmission of heat however can be achieved only by conduction, convention or radiation:

- **Conduction:** process applies primarily to heat transmission through solid materials. Metals are good conductor of heat, whereas non-metals in general are poor conductor or insulator. It is study deeply in the next section.
- **Convention:** process of transmitting heat through a fluid such a liquid or gas.
- **Radiation:** process by which heat is transferred through the motion of waves.

### 2.3.1 Heat conduction

On a microscopic scale, heat conduction occurs as rapidly vibrating atoms interacting with neighbouring atoms and transferring some of their energy (heat) to these neighbouring particles. The heat conduction occurs also with the movement of phonons, important in the case of graphite. These two mechanisms of propagation of heat are reduced by obstacles in the lattices due to impurities, additives, dislocations and other electrons or phonons. Conduction is the most

significant means of heat transfer within a solid or between solid objects in thermal contact. Fluids (especially gases) are less conductive than solids.

- Steady state conduction is a form of conduction that happens when the temperature difference driving the conduction is constant, so that after an equilibration time, the spatial distribution of temperatures in the conducting object does not change any further. In steady state conduction, the amount of heat entering a section is equal to amount of heat coming out. The heat conducted perpendicular to the heat flow can be stated by Fourier's law, the heat transfer per unit area in x direction is:

$$\frac{q_x}{A} = -k \cdot \frac{dT}{dx} \quad (9)$$

Where:

$q_x/A$ : Heat conducted per unit area perpendicular to the heat flow

$k$ : Thermal conductivity

$dT/dx$ : gradient of the temperature in two points through x direction

- Transient conduction occurs when the temperature changes as a function of time. Analysis of transient systems is more complex and often calls for the application of approximation theories or numerical analysis by computer. The heat equation is:

$$\frac{dT}{dt} = \alpha \cdot \frac{d^2T}{dx^2} + \frac{\dot{q}}{\rho c_p} \quad (10)$$

Where:

$dT/dx$ : gradient of the temperature in two points through the time

$d^2T/dx^2$ : second gradient of the temperature in two points through x direction

$\alpha$ : thermal diffusivity

$\dot{q}$ : heat source term

$\rho$ : density

$c_p$ : specific heat capacity

### 2.3.2 Thermal expansion

In the international units system it is measured as  $1/K$ . The thermal expansion is the tendency of solids to vary the volume when a change in temperature occurs. When a substance is heated, its atoms begin moving more and thus usually maintain a greater average separation. The degree of expansion divided by the change in temperature is called the material's coefficient of thermal expansion and generally varies with temperature.

### 2.3.3 Specific heat capacity

In the international units system it is measured as  $J/(kg \cdot K)$ . The specific heat is a physical quantity which is defined as the amount of heat to be supplied to the mass unit of a substance or thermodynamic system to raise its temperature in one unit (kelvin or degree Celsius). In general, the specific heat value depends of the initial temperature.

### 2.3.4 Thermal diffusivity

In the international units system it is measured as  $m^2/s$ . The thermal diffusivity characterizes the speed with which the temperature of the material varies with an application temperature, for example, to a sharp variation in surface temperature.

### 2.3.5 Thermal conductivity

Thermal conductivity is the physical property of any material which measures the ability of heat conduction there through. The inverse magnitude of the thermal conductivity is the heat resistance (ability of the material to resist the passage of heat). Thermal conductivity is a high capacity in metals in general and in continuous bodies and is lower in the gases to be very low in some materials such as fiberglass, so called, thermal insulators.

The coefficient of thermal conductivity ( $\lambda$  or  $k$ ) is measured in the international system as  $W/(m \cdot K)$ . It characterizing the amount of heat needed per  $m^2$ , so that, flowing during the time unit, 1 m of homogeneous material obtain a difference of  $1^\circ C$  between the two faces.

$$k = \rho \cdot c_p \cdot \alpha_D \quad (11)$$

Where:

k: thermal conductivity coefficient

$\rho$ : density

$\alpha_D$ : thermal diffusivity  
 $c_p$ : specific heat capacity

## 2.4 Treatments for cast iron

Although pure iron is a weak material, iron and carbon alloys cover a wide range of the strength spectrum from low yield stress levels (around 200 MPa) to very high levels (approaching 2000 MPa). These mechanical properties are usually achieved by the combined use of several strengthening mechanisms and in such circumstances it is often difficult to quantify the different contributions to the strength. Like other metals, iron can be strengthened by several basic mechanisms, the most important of which are

The heat treatments are cooling and heating operations at certain temperatures and conditions, that the cast irons and other alloys are subjected in order to give them features more suitable for their use. This operations change the crystal structure remaining unaltered composition of the material, they considerably alter the matrix microstructure with little or no effect on the size and shape of the graphite achieved during casting.

The ability to improve certain properties by tempering in cast irons is due to which these alloys when heated at elevated temperatures from 750 to 900 °C, almost one part is transformed, into austenite with FCC structure. This constituent then cooled more or less rapidly, becomes martensite with BCT structure as shown in Figure 13 or other intermediates.

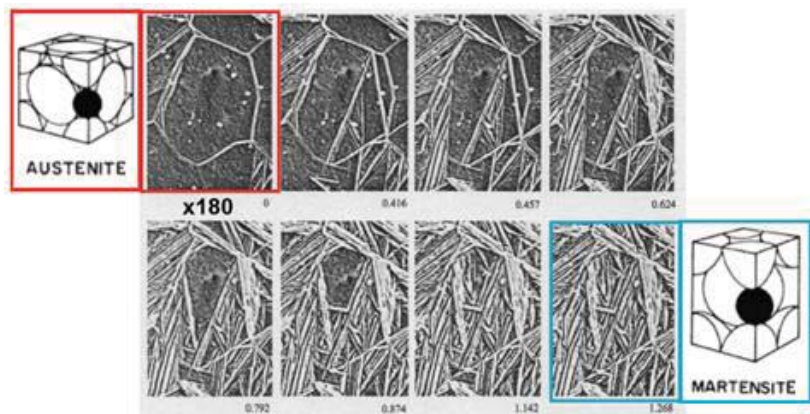


Figure 13. Transformation from austenite (FCC) to martensite (BCT) [14]

The martensite and the other intermediate constituents have properties of great interest for many applications. These properties are much better than those corresponding to the raw castings. In general, the laws governing the heat treatments of the cast irons are very similar to those of steels.

However, even though grey iron can be hardened by quenching from elevated temperatures, heat treatment is not ordinarily used commercially to increase the overall strength of grey iron castings because the strength of the as-cast metal can be increased at less cost by reducing the silicon and total carbon contents or by adding alloying elements as silicon or manganese. Next there is an explication of most common treatments for cast iron, mostly obtained from [15].

### **2.4.1 Annealing**

The annealing consists of heating the cast iron to a temperature high enough to make it softer with the advantage that its machinability is improved. This heat treatment reduces the mechanical properties of the cast iron, the reduction degree depends on the annealing temperature, the time at temperature, and the alloy composition of the iron. It is the most common heat treatment in grey cast iron and there are three different treatments each of which involves heating to a different temperature range: ferritizing, medium and graphitizing annealing:

- Ferritizing annealing: the temperature is raised to 700-760 °C and maintained a certain time, estimated as 1 hour per 25 mm thickness and then the cast iron is cooled in the oven with closed doors. Microstructurally this treatment ensures that pearlite matrix becomes ferrite and graphite obtaining a softer material.
- Medium annealing: it is used when previous treatment has not obtained the ferrite for whatever reason, like high alloys content or slow cooling parts in the material. In this case the temperature reached is 800-900 °C, above the eutectoid transformation temperature and holding ferritizing annealing times. After that, the casting is cooled slowly through the eutectoid transformation region, promoting the formation of ferrite. At these temperatures there is no formation of graphite or it is minimal. This treatment is recommended for grey cast iron castings with high hardness or containing cementite.
- Graphitizing annealing: the temperature reached is around 900-925 °C. It is used only when it is necessary remove the carbides. The highest heat time should be the minimum (to prevent oxidation and rusting in the grain boundaries). After decomposition of hydrocarbons, the way of cooling depends on the desired microstructure, for ferritic matrix, it is recommended a cooling in the oven with closed doors and for cast pearlitic matrix, it is recommended air cooling.

### **2.4.2 Stress relieving**

The goal of this treatment is to remove or reduce the internal stresses created in a metal and it has no effect on the mechanical properties. These internal stresses are caused for different reasons related with the cooling of the piece, like cold working or non-uniform cooling. It can be considered as an annealing treatment where the temperature reached is around 550 °C. This temperature is maintained for a period which depends on the constitution of the piece and casting. This period is generally considered equal to 1 hour per 25 mm thickness and then gives a cooling in the oven with closed doors. It must be employed slow speeds of heating and cooling especially to avoid new internal stresses or breaks in the piece. It is recommended to make this kind of annealing to parts of complicated shapes, or when dimensional tolerances must be very precise, as engine cylinders explosion or workshop tools tables.

### **2.4.3 Normalizing**

The pieces are heated to 850-950 °C and then cooling in still air at room temperature. In the case of grey cast iron, microstructurally, this treatment ensures a complete structural transformation of the ferritic-pearlitic or ferrite matrix in pearlite matrix. Normalization is used to increase the hardness, wear resistance and toughness of the casting and to restore the properties that have been modified by another heating process, such as welding.

### **2.4.4 Work hardening**

Work hardening is an important strengthening process in iron and carbon alloys, particularly in obtaining high strength levels in rod and wire, both in plain carbon and alloy steels. Without the addition of special alloying elements, these alloys can be raised to strength levels above 1500 MPa simply by the phenomenon of work hardening.

### **2.4.5 Solid solution strengthening**

Solid solution strengthening is a type of alloying that can be used to improve the strength of a pure metal. The technique works by adding atoms of one element (the alloying element) to the crystalline lattice of another element (the base metal). The alloying element diffuses into the matrix, forming a solid solution. Depending on the size of the alloying element, a substitutional solid solution or an interstitial solid solution can form. In both cases, the overall crystal structure is essentially unchanged.

- Substitutional solid solution strengthening: it occurs when the solute atom is large enough that it can replace solvent atoms in their lattice positions. According to the Hume-Rothery rules, solvent and solute atoms must differ in atomic size by less than 15% in order to form this type of solution. Because both elements exist in the same crystalline lattice, both elements in their pure form must be of the same crystal structure.

Many metallic elements form solid solutions in  $\gamma$ -iron and  $\alpha$ -iron. For a constant atomic concentration of alloying elements there are large variations in strength. The relative strengthening might alter with the temperature of testing and with the concentrations of interstitial solutes present in the irons. Strengthening elements are silicon, molybdenum, phosphorus, manganese, nickel and copper.

- Interstitial solid solution strengthening: it occurs when the solute atom is equal or larger than the solvent atoms. The atoms crowd into the interstitial sites, causing the bonds of the solvent atoms to compress and thus deform. The formation of interstitial atmospheres at dislocations requires diffusion of the solute. Carbon and nitrogen are examples of interstitial solid solution in iron. As both, carbon and nitrogen, diffuse much more rapidly in iron than substitutional solutes.

#### **2.4.6 Grain-boundary strengthening**

Grain-boundary strengthening (or Hall–Petch strengthening) is a method of strengthening materials by changing their average grain size. It is based on the observation that grain boundaries impede dislocation movement and that the number of dislocations within a grain have an effect on how easily dislocations can traverse grain boundaries and travel from grain to grain. So, by changing grain size one can influence dislocation movement and yield strength. The refinement of the grain size of ferrite provides one of the most important strengthening routes in the heat treatment of iron and carbon alloys.

### **2.4.7 Dispersion strengthening**

In all iron and carbon alloys there is normally more than one phase present, even sometimes several phases can be recognized in the microstructure. The matrix, which is usually ferrite with BCC structure or austenite with FCC structure, often is strengthened by controlling the dispersions of the other phases in the microstructure. In cast irons the commonest other phases are carbides (graphite) formed as a result of the low solubility of carbon in  $\alpha$ -iron. Most dispersions lead to strengthening, but often they can have adverse effects on ductility and toughness. The ideal case to perform this method is, for example after tempering, when in cast irons, the structure consists of spheroidal cementite particles in a ferritic matrix. However, they can provide approximations in less ideal cases.

## 3 Method and implementation

### 3.1 Materials

Five cast irons with different compositions presented mainly in Table 2 (the complete components analysis table is attached in appendix 1) were casted on SKF (Katrineholm, Sweden) in five grades with six plates each one with thicknesses of 3, 7, 15, 30, 50 and 75 mm each one as shown in Figure 14.

Table 2. Main components analysis of each casting

Element	G82B SGI	G88 SGI	G89 SGI	G88 CGI	G89 CGI
C	3.51	3.28	3.13	3.24	3.18
Si	2.36	3.73	4.25	3.44	3.87
Mn	0.408	0.169	0.169	0.17	0.167
P	0.0063	0.009	0.0095	0.0069	0.0072
S	0.0043	0.0056	0.0065	0.0062	0.0072
Cr	0.025	0.028	0.029	0.028	0.028
Ni	0.039	0.045	0.041	0.048	0.047
Mo	0.0028	0.0012	0.0016	0.0034	0.0037
CE	4.30	4.53	4.55	4.39	4.47

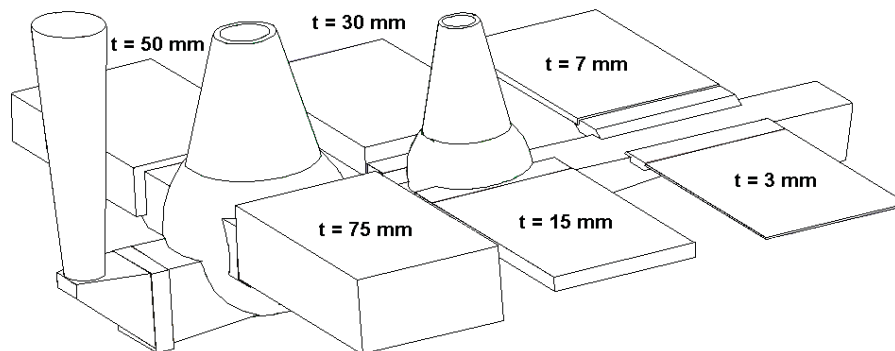


Figure 14. Casting pattern

In order to have an idea of the thermal conductivity of each casting the plates chosen to study in this project and the thicknesses of the plates were:

- SGI G82B (15, 50 and 75 mm)

- SGI G88 (50 mm)
- SGI G89 (15, 50 and 75 mm)
- CGI G88 (50 mm)
- CGI G89 (15, 50 and 75 mm)

The process to obtain the samples was the same for all the different plates in order to obtain a microstructure as same as possible. The piece of each plate given for this project was 30 mm from the outside and the surface approximate 5 mm of each plate were avoided due to the different solidification structure compared to the rest of the plate. A squared section prism was cut, and after, using the lathe, a perfect cylinder was obtained. Finally the thickness of the samples was adjusted with the grinder. As shown in Figure 15, after avoid the surface material, the first samples processed from this cylinder were DSC samples (0.5 mm of thickness and 4 mm of diameter), after the dilatometer samples (12 mm of thickness and 6 mm of diameter) and finally the laser flash samples (4.5 mm of thickness and 12.5 mm of diameter). All the dimensions have a tolerance of  $\pm 0.1$  mm.

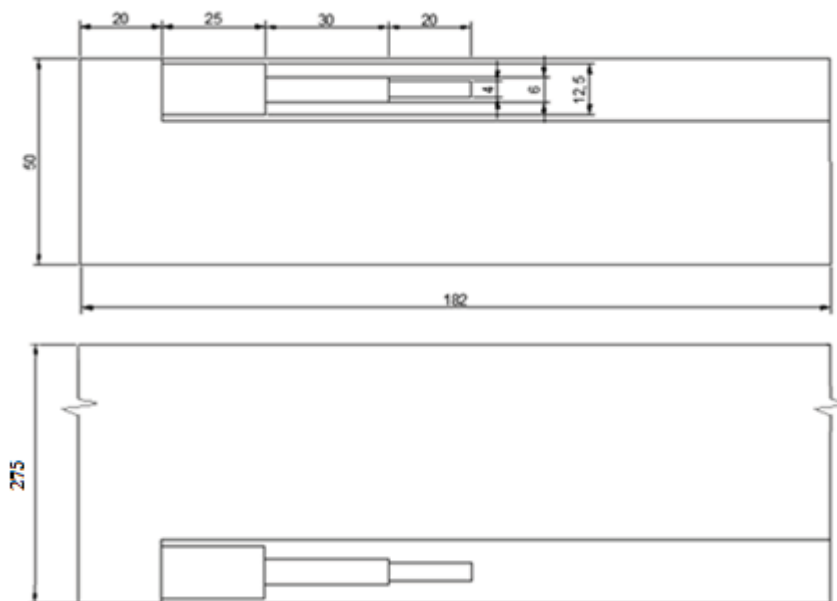


Figure 15. Situation of the samples in the 50 mm plate (units: millimetres)

It is known that the thermal conductivity of cast irons varies with the temperature. In this project, the thermal conductivity of the different studied cast irons was calculated from room temperature to 500 °C and after the nodularity of each casting was studied. Three experiments explained below were realized, dilatometer, Differential scanner calorimetry (DSC), Laser flash and also and in order to obtain the density of the castings at higher temperatures than room temperature it was calculated the thermal expansion from the dilatometer results

and the density at room temperature. When all the required data was evaluated, the thermal conductivity of each casting was calculated using the expression:

$$k(T) = \rho(T) \cdot c_p(T) \cdot \alpha_D(T) \quad (12)$$

Where:

k: thermal conductivity coefficient at temperature T

$\rho$ : density at temperature T

$\alpha_D$ : thermal diffusivity at temperature T

$c_p$ : specific heat capacity at temperature T

## 3.2 Dilatometer

Dilatometry is an experiment used to measure the variation on the dimensions of one sample, both expansion and shrinkage, under a known load and subjected to a controlled temperature and time program. In dilatometry the samples studied can be solids, powders, pastes and liquids, but in this project all the samples studied are on solid state. The combination of dilatometry with calculated Differential Thermal Analysis (c-DTA®) allows thermal expansion measurements of the samples. The equipment used in the laboratory was the Netzsch Dilatometer 402C equipped with Proteus analysis software.



Figure 16. Netzsch Dilatometer 402C [19]

To perform a dilatometric analysis, the sample is inserted into a special holder within a movable furnace. A pushrod is positioned directly against the sample and transmits the length change to a linear variable displacement transducer (LVDT). As the sample length changes during the temperature program, the LVDT core is moved and an output signal proportional to the displacement is recorded. The temperature program is controlled using a thermocouple located next to the sample. Since the sample holder and the front part of the pushrod are being

exposed to the same temperature program as the sample, they are also expanding. The resulting dilatometer signal is therefore the sum of the length changes of sample, sample holder and pushrod. It is thus necessary to correct the raw dilatometer data in order to obtain a true view of sample behaviour [19].

The dilatometer samples had cylindrical shape with 6 mm of diameter and 12 mm of length with a tolerance of  $\pm 0.1$  mm. The experiment was realized inside the chamber, in a Helium overpressure atmosphere in order to prevent oxidation in the sample. The chamber was vacuumed and filled of Helium three times in order to sure the pureness of the environment.

First a standard measuring is done in order to calibrate the next measurements, in this case an aluminium oxide sample with same dimensions than the samples that were going to be studied after. This standard measurement is used as base in the rest of the samples experiments. The sample was heated to 500 °C with a heating ratio of 5 K/min and then cooling to room temperature again. While the experiment was running, the software created the graphic with the relation between the relative elongation of the sample and the temperature which typical shape is shown in Figure 17, where red curve is heating process and blue curve is cooling curve.

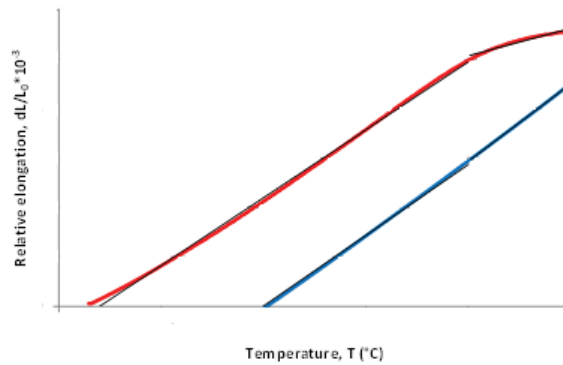


Figure 17. Result of dilatometer experiment

The lineal thermal expansion value for one single temperature is represented as the slope of the curve in that point and it was determined by the expression:

$$\alpha_E = \left( \frac{\Delta L}{\Delta T} \right) \frac{1}{L_0} \quad (13)$$

Where:

$\alpha_E$ : lineal thermal expansion coefficient

$\Delta L$ : change in length

$\Delta T$ : change in temperature

$L_0$ : initial sample length

As shown in Figure 17 the heating curve slope is not constant, approximately at 400 °C it is modified, because the thickness of the sample increases when it is heated. If  $L_T$  is the thickness of the sample at temperature  $T$ , the equation of the thickness is different between the ranges of temperature from room temperature to 400 °C and from 400 to 500 °C, for the heating curve approximation, the lines equations are:

$$\text{From RT to 400 °C: } L_{RT-400^{\circ}\text{C}} = L_0 + L_0 \cdot \alpha_E \cdot (T - T_{RT}) \quad (14)$$

$$\text{From 400 to 500 °C: } L_{400-500^{\circ}\text{C}} = L_{400^{\circ}\text{C}} + L_{400^{\circ}\text{C}} \cdot \alpha_E \cdot (T - T_{400^{\circ}\text{C}}) \quad (15)$$

### 3.3 Archimedes' principle

Archimedes' principle is a law of physics stating that the upward force exerted on a body immersed in a fluid is equal to the weight of the fluid the body displaces. The density of the immersed object can easily be calculated without measuring any volumes, applying the Archimedes' principle.

In this project, the weight of each sample was measured inside and outside a glass with distilled water and the density at room temperature was calculated with this expression:

$$\rho_{RT} = \frac{m_{air}}{m_{air} - m_{H_2O}} \cdot \rho_{H_2O} \quad (16)$$

Where:

$\rho_{RT}$ : density of the sample at room temperature

$m_{air}$ : weight of the sample measured in the air

$m_{H_2O}$ : weight of the sample measured in the water

$\rho_{H_2O}$ : density of the water at room temperature. ( $\rho_{H_2O}=1 \text{ g/cm}^3=1000 \text{ kg/m}^3$ )

The density of the materials varies with the temperature, in this project this expression is used in order to get acceptable approximations of the densities at high temperatures of cast irons:

$$\rho = \frac{\rho_{RT}}{1+3 \cdot \alpha_E \cdot (T-T_{RT})} \quad (17)$$

Where:

$\rho$ : density at temperature T

$\rho_{RT}$ : bulk density of the sample at room temperature

$\alpha_E$ : lineal thermal expansion

T: temperature of the sample

$T_{RT}$ : room temperature

For this project the density of each casting was measured with the equipment Kern ABJ shown in Figure 18, based on the Arquimedes` principle. The samples were put in the water carefully to avoid the bubble attachment on the surface of the samples.



Figure 18. Kern ABJ

### 3.4 Differential Scanning Calorimetry (DSC)

The DSC experiment is used to obtain the specific heat of the studied cast irons. The equipment used in the laboratory was the Netzsch DSC 404 C Pegasus shown in Figure 19 equipped with Proteus software. This equipment can obtain besides the specific heat capacity, enthalpies, phase diagrams, purity, crystallization, glass transitions, reaction kinetics, etc.



Figure 19. Netzsch DSC 404 C Pegasus [19]

The dimensions of the samples used in these experiments are 4 mm of diameter and 0.5 mm of thickness with a tolerance of  $\pm 0.1$  mm. Before the experiment, the samples were cleaned in acetone and after dried with hot air.

The experiment started setting the atmosphere of the chamber, first doing the evacuating and then filling it with Argon. This process is repeated three times in order to sure the pureness of the environment inside the chamber. After this process the measurements are done in a continuous Argon flow with rate of 50 ml/min.

In this experiment the sample and a reference sapphire standard with same dimensions, 42.1 mg of weigh and known specific heat. The samples were subjected to a controlled temperature program, heating to 500 °C and cooling to room temperature. The heating and cooling rate is 10 K/min. The actual measured properties are the temperature of the sample and the temperature difference between sample and reference. From the raw data signals, the heat flow difference between sample and reference can be determined using heat flux principle. The DSC thermo analysis consists of three measurements:

- Correction: both crucibles are empty. A correction from thermal gradients in the furnace is made.
- Standard: the inner crucible is empty and the sapphire is placed in the outer crucible.
- Sample: the inner crucible is empty and the studied sample is placed in the outer crucible.

The analysis of the results was done by Proteus software and the specific heat was calculated with the  $c_p$  ratio method. In this project, the  $c_p$  of each casting was measured in both, heating and cooling processes.

### **3.5 Laser Flash method**

There are two main techniques to measure the thermal diffusivity of a material: guarded heat flow meter and the method used on this project, the Laser flash method, deeply explained in the paper [20]. The equipment employed was the Netzsch LFA 427 shown in Figure 20. It is the most common method due to it is a non-contact, non-destructive method and no additional safety precautions are necessary.



Figure 20. Netzsch LFA 427 [19]

The dimensions of the samples used in this method are 12.5 mm of diameter and 4.5 mm of thickness, with a tolerance of  $\pm 0.1$  mm and before the experiment, the samples were roughen with an air sand gun in order to obtain a rear non-reflective surface. Before the experiment, the samples were cleaned with acetone and dried with hot air. After this process, the samples were mounted on a holder inside the equipment furnace. When the samples were inside the chamber, the air inside it was evacuated and the chamber was filled with a continuous 100 ml/min Argon flow. After the sample reached a predetermined temperature, a burst of energy emanating from a pulsed laser is absorbed on the front face of the sample, resulting in homogeneous heating. The laser voltage used was 450 V and the pulse with was 0.8 ms. The relative temperature increase on the rear face of the sample is then measured as a function of time by an IR detector. The thermal diffusivity is computed by the software using these time/relative temperature increase data. The process is shown in Figure 21. For adiabatic conditions, the thermal diffusivity is determined by the equation:

$$\alpha_D = 0.1388 \cdot \frac{L^2}{t_{0.5}} \quad (18)$$

Where:

$\alpha_D$ : thermal diffusivity

L: sample thickness

$t_{0.5}$ : time at 50% of the temperature increase.

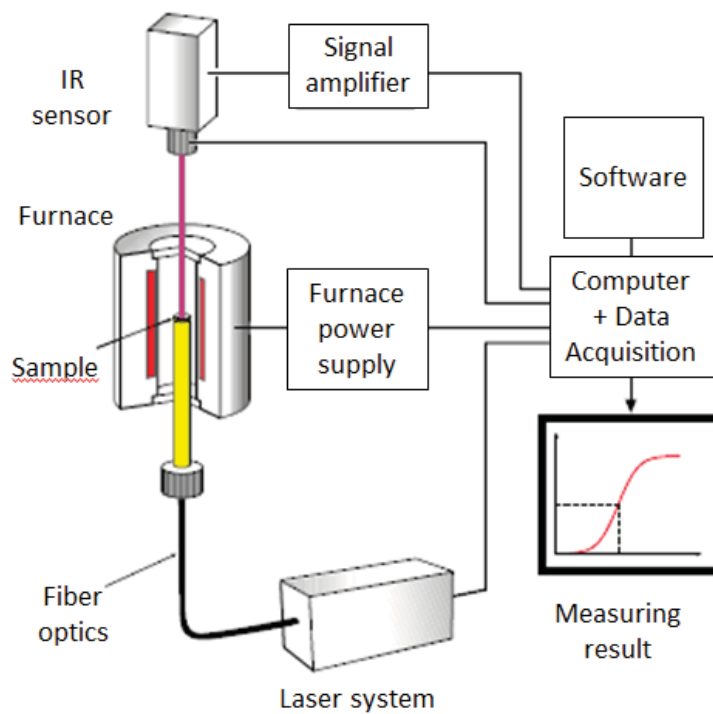


Figure 21. Laser flash method [19]

In the present study, measurements have done five times at each temperature 25, 100, 200, 300, 400 and 500 °C. The heating rate was 10 K/min. In order to obtain a better accuracy, a diffusivity correction called radiation plus pulse correction was applied to the laser method diffusivity results in order to obtain a correlation coefficient always higher than 0.99. The experiment is done taking constant thermal expansion and that is why a second correction explained on next chapter is applied to the results obtained from Laser Flash method.

### 3.6 Samples preparation and optical microscope

The cast samples were mounted in a baquelite holder with cylindrical shape as shown in Figure 22, with the equipment Struers Citopress shown in Figure 23. It works as a press, placing the sample surrounded with baquelite powder in a cylindrical chamber, heating it and increasing the pressure in order to compact the powder and obtaining the wished sample.



Figure 22. Samples mounted in a baquelite cylinder



Figure 23. Struers Citopress [21]

The new samples were polished in the equipment Struers Tegramin shown in Figure 24. The goal was obtaining a reflecting surface in order to be analysed in the microscope. The polish program applied to the samples was the standard for cast iron material consisting on three phases. The first phase consisted on sandpaper Piano 220 and suspension liquid water for one minute, with a pressure of 35 Nw. the second phase consist on sandpaper Largo 9 and suspension liquid diamond for three minutes, with a pressure of 35 Nw and the third phase consist on paper DAC and suspension liquid diamond for three minutes, with a pressure of 35 Nw.



Figure 24. Struers Tegramin [21]

The equipment used to analyse the nodularity of the samples was an optical microscope Leica Leitz DMRX connected to the Leica Qwin v3 software. The magnification used was 1.0x on the microscope, 10x on the objective lenses and 10x on the eyepiece lenses, multiplying this factors the increasing obtained was of 100x. The nodularity was measured with a program based on the SinterCast standard, being the parameters introduced to accept a shape as carbon minimum area of  $20 \mu\text{m}^2$  and minimum length of  $10 \mu\text{m}$ . Forty pictures were taken of each sample covering in total a surface bigger than  $10 \text{mm}^2$  around the entire surface, in order to obtain a representative average of the real nodularity of each cast iron.

The samples were treated with nylol 5% and the same microscope was used with the same magnification in order to take pictures of the matrices. Twenty pictures were taken of each sample covering in total a surface bigger than  $5 \text{mm}^2$  around the entire surface, in order to calculate with the software a representative average of the real ferrite and pearlite amount of each cast iron.

## 4 Findings and analysis

### 4.1 Thermal expansion

The thermal expansion values used in this project were the slopes of the curves obtained from dilatometer experiment which was performance one per sample. These values are shown in Table 3 and the real curves obtained from the dilatometer are plotted together with the line approximations in appendix 2.

Table 3. Thermal expansion values,  $\alpha_E / 10^{-6} \cdot K^{-1}$

	Heating		Cooling	
	RT-400 °C	400-500 °C	RT-400 °C	400-500 °C
<b>G82B SGI 15mm</b>	13.33	5.93	14.18	15.70
<b>G82B SGI 50mm</b>	14.04	13.43	14.61	16.05
<b>G82B SGI 75mm</b>	14.32	14.48	15.00	16.25
<b>G88 SGI 50mm</b>	13.38	7.36	14.55	15.83
<b>G89 SGI 15mm</b>	13.96	13.60	14.29	15.59
<b>G89 SGI 50mm</b>	14.04	10.70	14.95	15.64
<b>G89 SGI 75mm</b>	13.12	11.74	13.94	15.15
<b>G88 CGI 50mm</b>	14.10	13.08	13.95	15.30
<b>G89CGI 15mm</b>	13.75	11.50	14.07	15.48
<b>G89 CGI 50mm</b>	14.46	13.43	14.93	15.96
<b>G89 CGI 75mm</b>	13.20	11.41	14.81	15.83

For all the studied cases in the heating process the slope is higher in the range from room temperature to 400 °C than in the range between 400 and 500 °C. In the cooling process otherwise the slope is higher from 400 to 500 °C than from room temperature to 400 °C range.

## 4.2 Specific heat capacity

Due to the cooling rate is decreased from the 15 mm to the 75 mm plates, the results of the DSC experiment are plotted in the same graphic for the three thicknesses of same casting in order to study how the cooling rate affect the thermal conductivity of one cast iron. Results of casting G82B SGI are shown in Figure 25, of casting G89 SGI on the Figure 26 and of casting G89 CGI on the Figure 27. In all the graphics the red curve represents the 15 mm of thickness plate, the green curve the 50 mm plate and the purple curve the 75 mm plate.

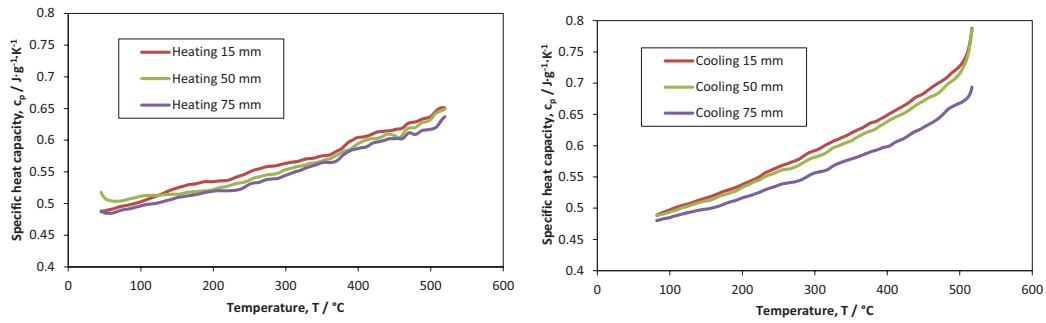


Figure 25.  $c_p$  results for three thicknesses of casting G82B SGI for both, heating (left) and cooling (right) processes

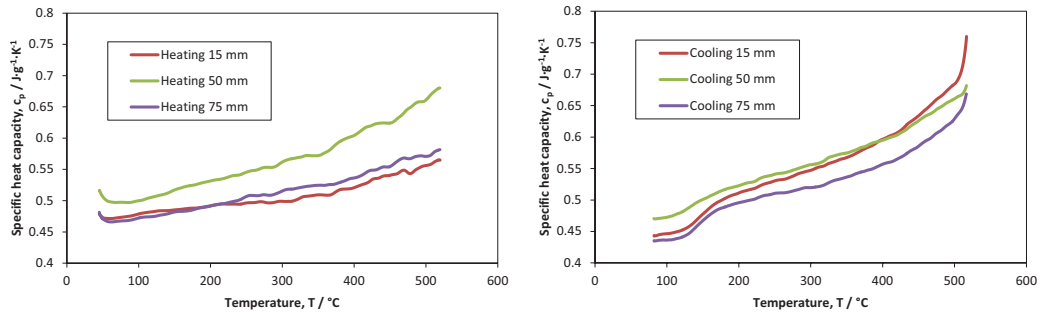


Figure 26.  $c_p$  results for three thicknesses of casting G89 SGI for both, heating (left) and cooling (right) processes

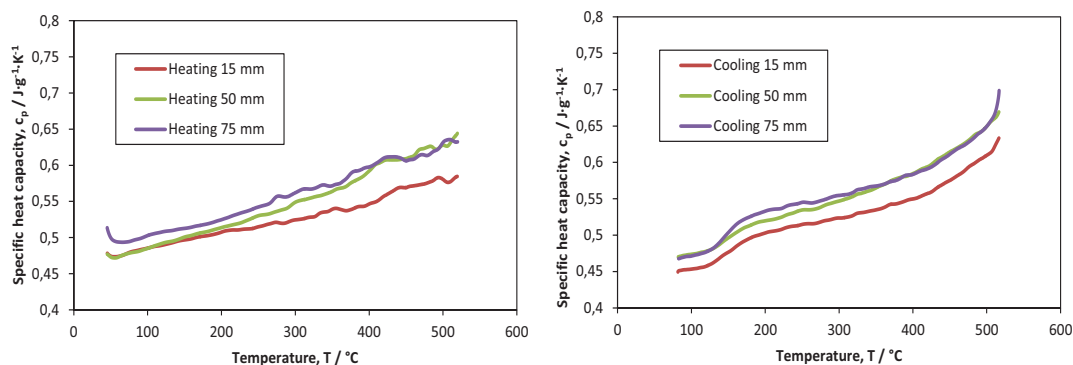


Figure 27.  $c_p$  results for three thicknesses of casting G89 CGI for both, heating (left) and cooling (right) processes

The results of the DSC experiment are also compared for the castings with different content of silicon in order to analyse the possible thermal differences due to the inoculation of this element. The results correspond to 50 mm of thickness plates in all the cases. In the case of SGI, the results for G82B SGI are represented with the red curve, G88 SGI with the blue curve and G89 SGI with the green curve and they are plotted together in Figure 28. In the case of CGI, the results are presented on Figure 29, being the results of G89 CGI the red curve and the results of G88 CGI the blue curve.

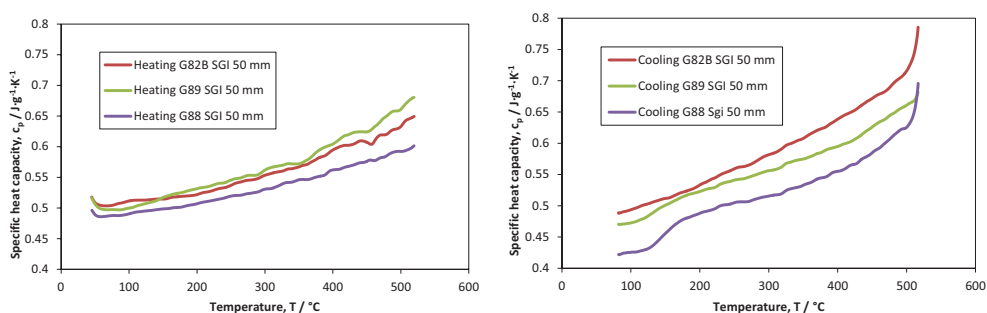


Figure 28.  $c_p$  results for three different silicon content castings G82B SGI, G88 SGI and G89 SGI for both, heating (left) and cooling (right) processes

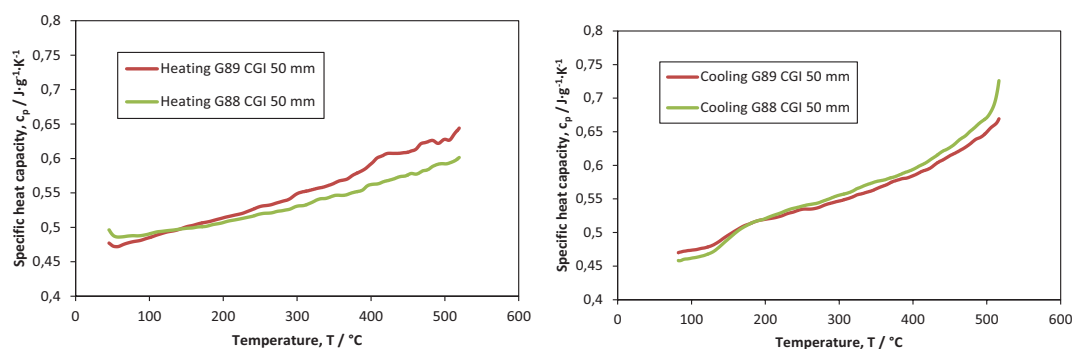


Figure 29.  $c_p$  results for two different silicon content castings G88 CGI and G89 CGI for both, heating (left) and cooling (right) processes

### 4.3 Thermal diffusivity

In the case of diffusivity the results were not obtained for each temperature, as explained above it was studied for RT, 100, 200, 300, 400 and 500  $^{\circ}C$ . That is why the results are exposed like points and not curves as  $c_p$  results. Although the error bar is presented for each point, this bar is calculated below and above the point with the standard deviation. This bar means that the point is not the exactly thermal diffusivity at this temperature and could be on this bar range. The results of the Laser flash method are shown in the same graphic for the three thicknesses of same cast iron as in DSC results in order to compare and analyse the possible thermal differences between plates of same castings with different thickness. Results of casting G82B SGI are shown in Figure 30, of casting G89 SGI in the Figure 31 and of casting G89 CGI in the Figure 32.

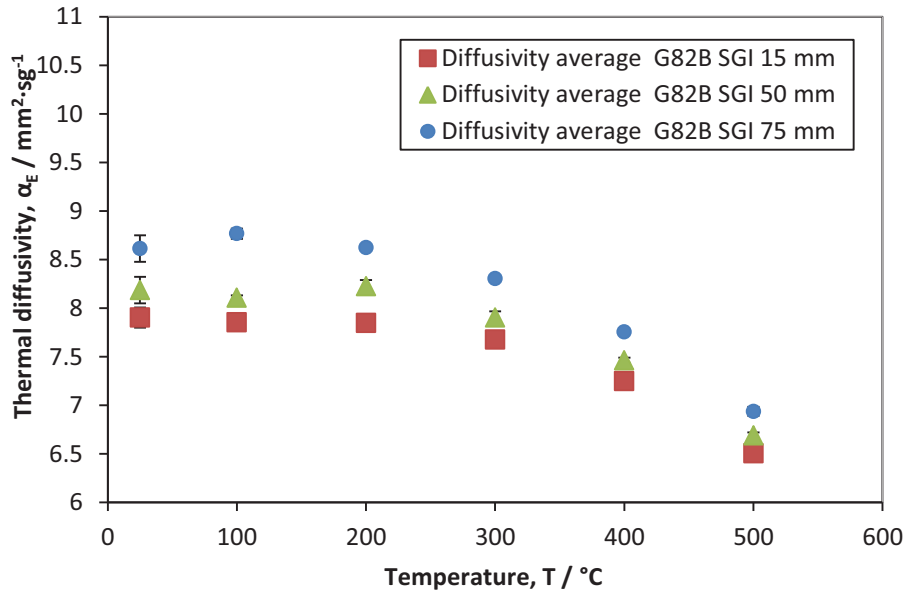


Figure 30. Thermal diffusivity of casting G82B SGI for the three thicknesses 15, 50 and 75 mm of plate

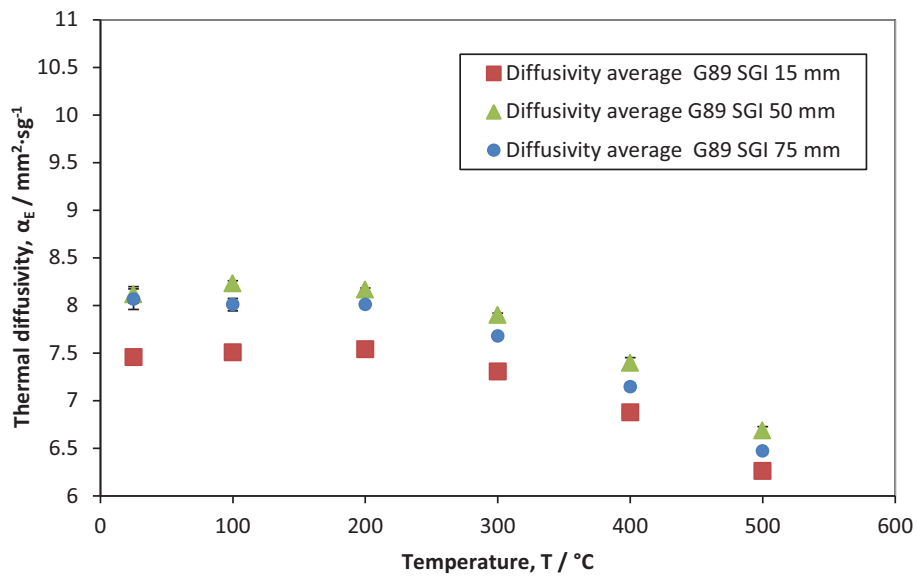


Figure 31. Thermal diffusivity of casting G89 SGI for the three thicknesses 15, 50 and 75 mm of plate

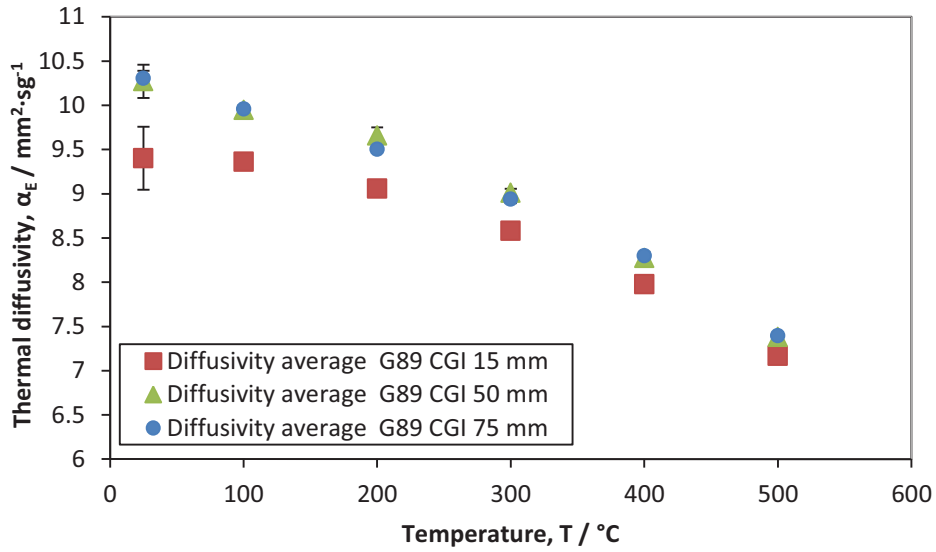


Figure 32. Thermal diffusivity of castings G89 CGI for the three thicknesses of plate 15, 50 and 75 mm

The results of the Laser Flash method are also compared for the castings with different content of silicon in order to analyse the possible thermal differences due to the inoculation of this element. The results correspond to 50 mm of thickness plates in all the cases. In the case of SGI the results are shown in Figure 33 and in the case of CGI the results are shown in Figure 34.

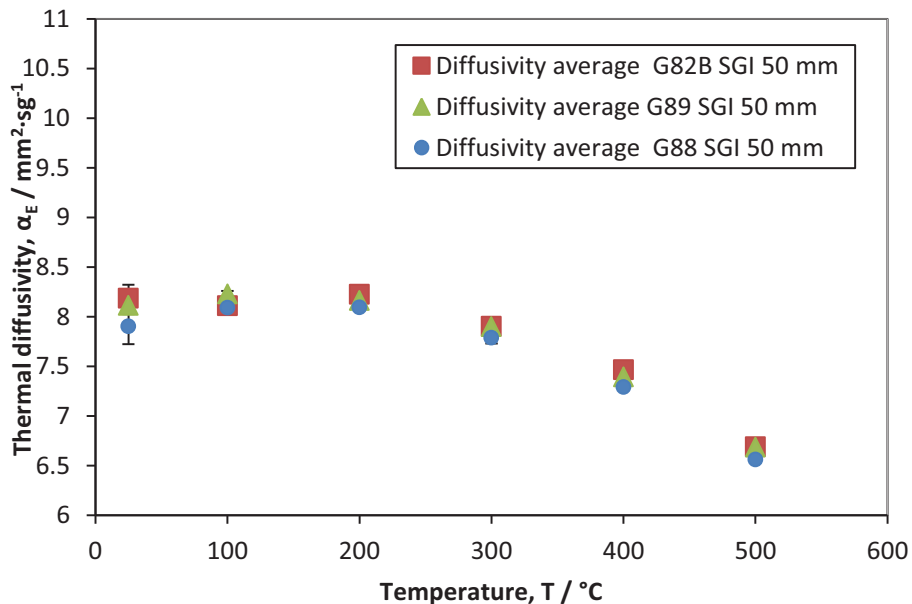


Figure 33. Thermal diffusivity results for three different silicon content castings G82B SGI, G88 SGI and G89 SGI

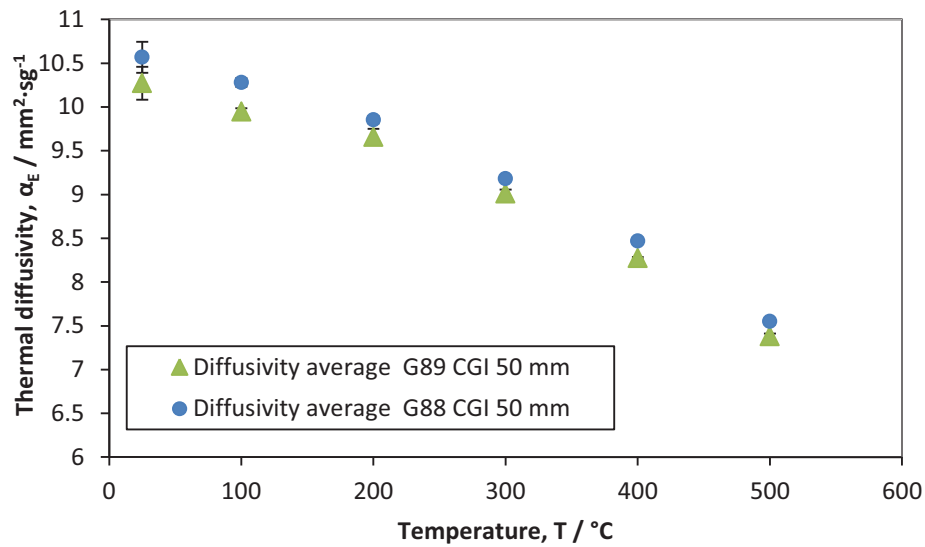


Figure 34. Thermal diffusivity results for two different silicon content castings G88 CGI and G89 CGI

#### 4.4 Thermal conductivity

The thermal conductivity values were calculated for all the studied castings and all these tables are attached to the report in the appendix 3. Below are presented the final results of the thermal conductivity of each casting following the above format, first are showed the graphs where three different thicknesses plates of same casting are compared, then the casting with different silicon are compared. Consider that the thermal conductivity values are calculated at 25, 100, 200, 300, 400 and 500 °C. These points are shown joined by straight lines so the sections between the calculated points show an approximate value of thermal conductivity at the corresponding temperatures. Results of casting G82B SGI are shown in Figure 25, of casting G89 SGI on the Figure 36 and of casting G89 CGI on the Figure 37. In all the graphics the red curve represents the 15 mm of thickness plate, the green curve the 50 mm plate, and the purple curve the 75 mm plate.

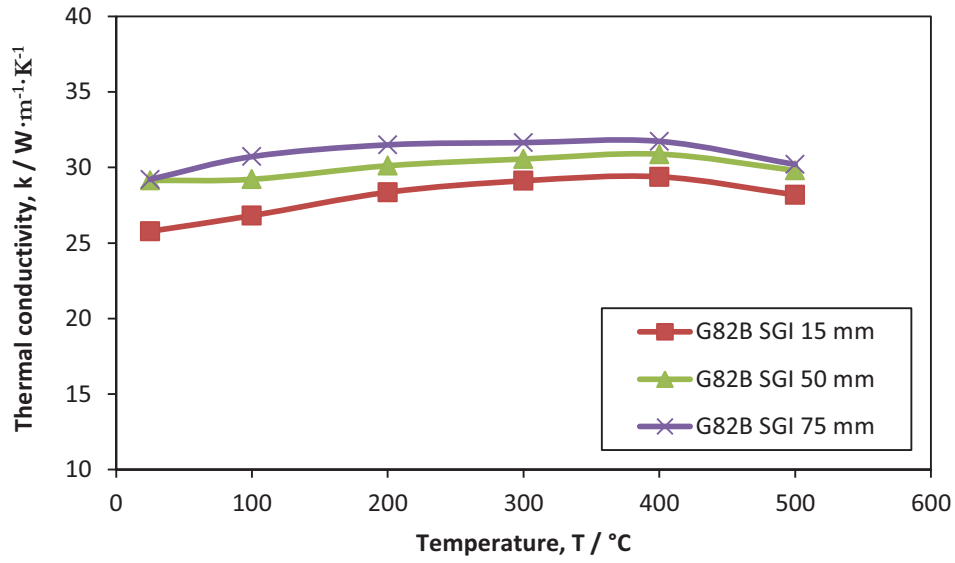


Figure 35. Thermal conductivity of casting G82B SGI for the three thicknesses 15, 50 and 75 mm of plate

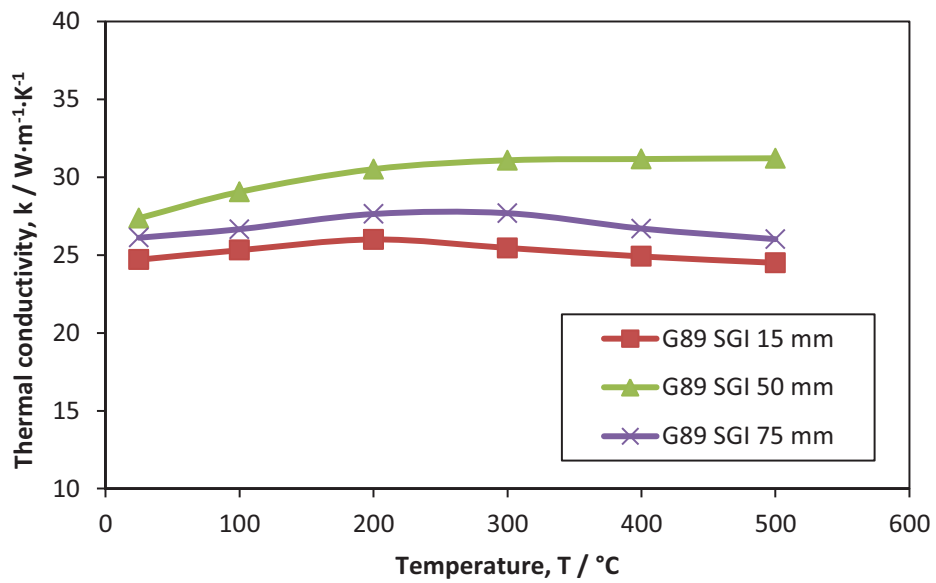


Figure 36. Thermal conductivity of casting G89 SGI for the three thicknesses 15, 50 and 75 mm of plate

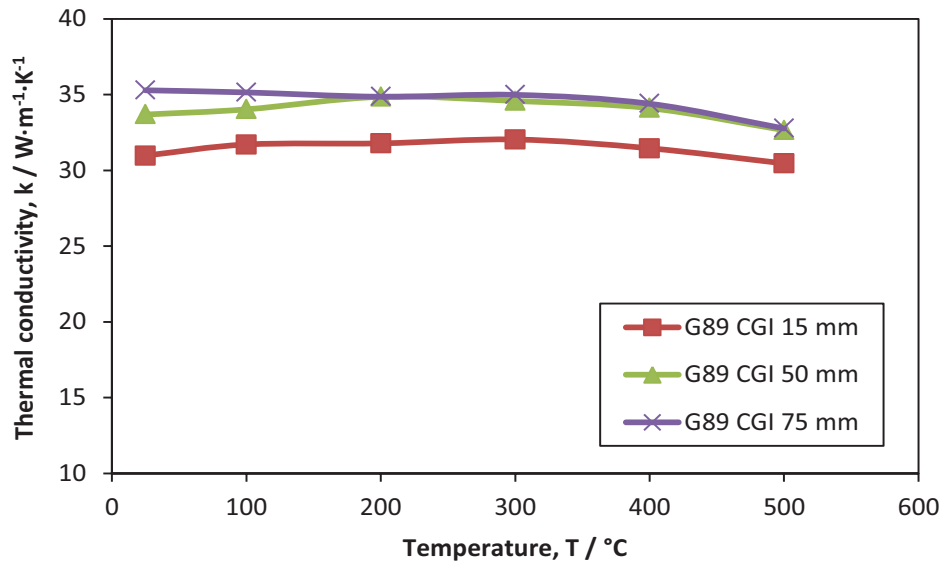


Figure 37. Thermal conductivity of casting G89 CGI for the three thicknesses 15, 50 and 75 mm of plate

The thermal conductivities of the same cooling rate castings are shown in in order to detect any relation between the thermal conductivity and the cooling ratio. The Figure 38 shows the thermal conductivity of the 15 mm castings and the Figure 39 shows the thermal conductivity of the 75 mm castings.

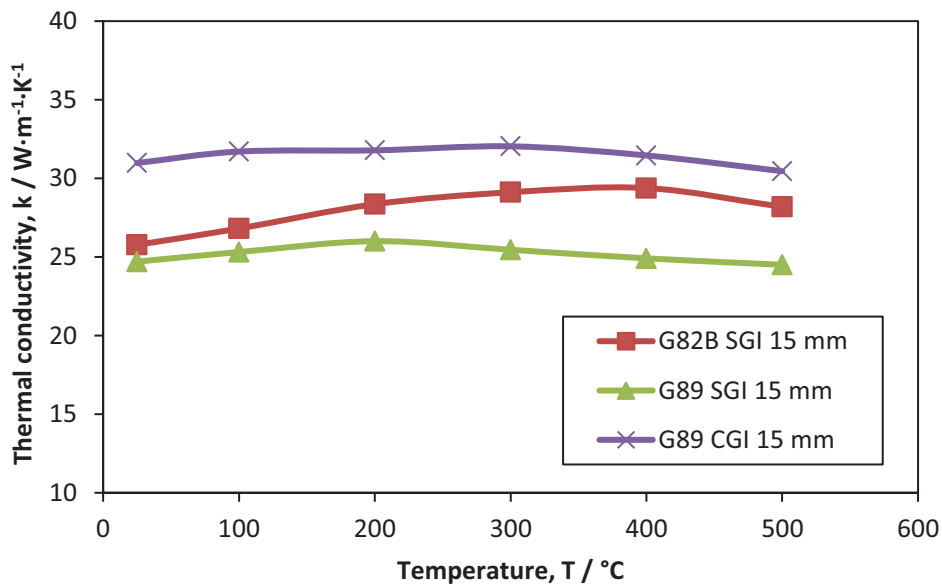


Figure 38. Thermal conductivity of 15 mm of thickness castings

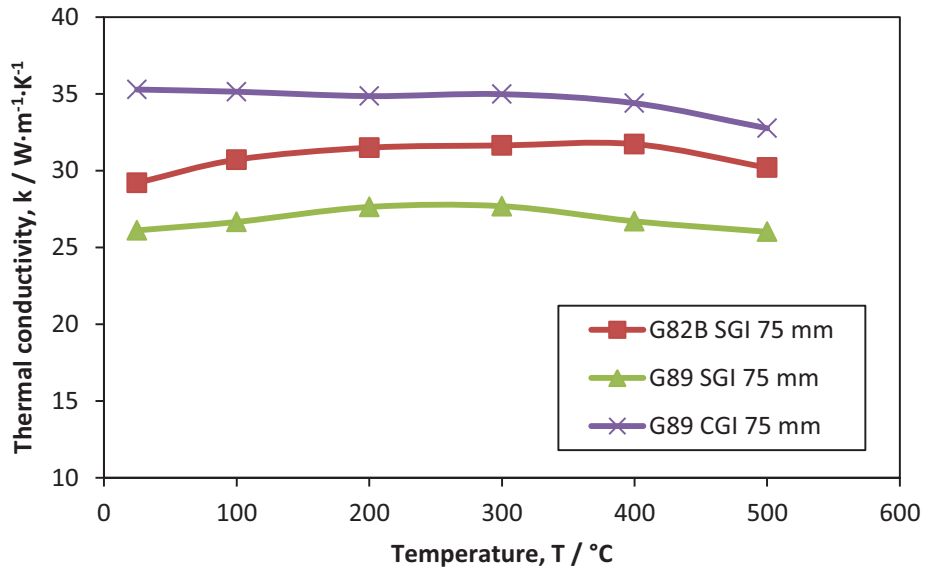


Figure 39. Thermal conductivity of 75 mm of thickness castings

Below are showed the results of different silicon content castings. In the case of SGI the results for G82B SGI are represented with the red curve, G88 SGI with the blue curve and G89 SGI with the green curve and these results are plotted together on Figure 28. In the case of CGI the results are presented on Figure 29, being the results of G89 CGI the red curve and the results of G88 CGI the blue curve. The results correspond to 50 mm of thickness plates in all the cases.

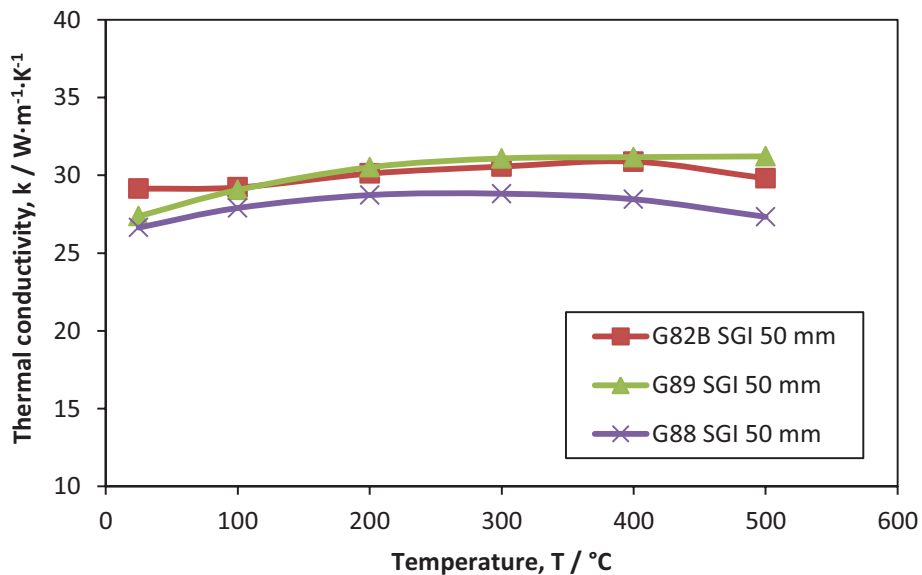


Figure 40. Thermal conductivity results for three different silicon content castings G82B SGI, G88 SGI and G89 SGI

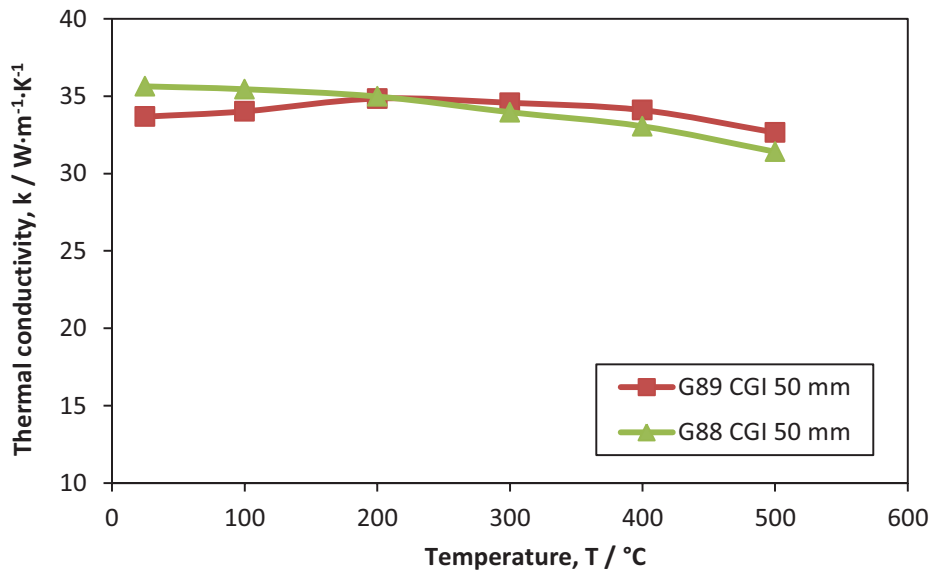


Figure 41. Thermal conductivity results for two different silicon content castings G88 CGI and G89 CGI

The results of the thermal conductivity obtained in this project show the form of the curves studied in other reports as [22]. The thermal conductivity of cast irons decreases when increasing the temperature.

- The thermal conductivity of grey cast irons increases as the amount of free graphite increases and as the flakes become coarser and longer. It is not study in this report but the thermal conductivity values of grey cast iron are the highest.
- The thermal conductivity of spheroidal graphite iron (SGI) is considerably lower than thermal conductivity of grey cast iron. In SGI the thermal conductivity is higher in ferritic matrix than in pearlitic matrix, and for quenched and tempered irons the values are in the middle. Thermal conductivity curve of SGI usually has a maximum point at 200-400 °C.
- Typical values for the thermal conductivity curve of compacted graphite iron (CGI) are between the grey cast iron thermal conductivity and the SGI thermal conductivity curves. Sometimes in CGI the curve raises a maximum at 200-300 °C as in SGI, but it doesn't occur always.

## 4.5 Nodularity

Two pictures of all the cast irons were taken, one of the graphite and the other of the matrix, all of them are in appendix 4. The nodularity of the castings was studied to have more knowledge of the material and have more sources in order

to explain the variations in the thermal properties. The results of the nodularity calculated with the software Leica Qwin v3 is presented in the Table 4.

Table 4. Nodularity (%) of all the studied castings and thicknesses

<b>Thickness</b>	<b>G82B SGI</b>	<b>G88 SGI</b>	<b>G89 SGI</b>	<b>G88 CGI</b>	<b>G89 CGI</b>
<b>15 mm</b>	75.42	-	30.68	-	17.04
<b>50 mm</b>	74.85	66.44	55.62	15.68	7.33
<b>75 mm</b>	82.62	-	53.74	-	3.92

The results of the nodularity for the castings G82B SGI are around the expected 80% while the results for the castings G88 and G89 SGI are lower, especially in the case of G89 SGI. For this casting the same result is detected in other project and this is probably due to a problem in the G89 SGI melt mixing. The results of the nodularity for the castings G88 and G89 CGI are in the expected range of 0-20%, being the nodularity of G88, with lower amount of silicon, higher than of G89 for the same cooling rate.

Furthermore, following the study of paper [23] where thermal conductivity of compact and spherical irons was related to nodularity and in which it is stated that there is a linear relationship between this properties when the casting was solidified to low ratio. The graph showing the thermal conductivity versus nodularity at room temperature is presented on Figure 42 where seems the castings with the cooling rate corresponding to a 50 mm thickness adjust better to the linear relationship than the casting cooled at the other rates.

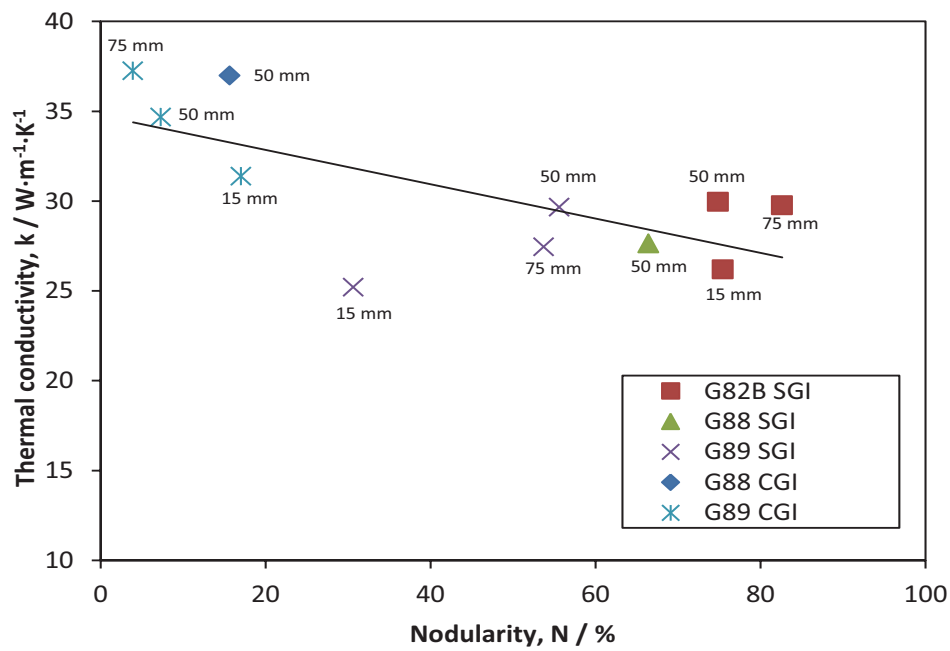


Figure 42. Thermal conductivity versus nodularity at room temperature

The Figure 43 shows the relation between the ratio cooling and the nodularity for all the studied cases. For the same cooling rate corresponding to a thickness of 50 mm. in the case of SGI the G88 SGI has higher nodularity than the G89 SGI while the G82B SGI has higher nodularity than the G88 SGI. In the case of CGI the G88 CGI has also higher nodularity than the G89 CGI. The castings with lower silicon content have higher nodularity than the castings with higher silicon for the same cooling rate.

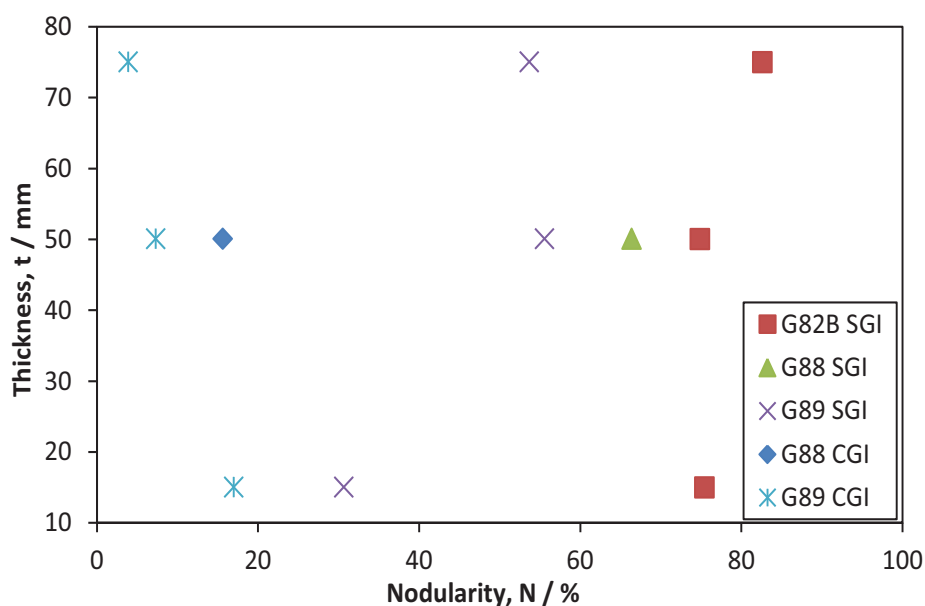


Figure 43. Thickness versus nodularity at room temperature

## 4.6 Graphite and matrix amount

The results of the graphite amount were obtained from the nodularity results and were used to calculate the ferrite and pearlite amount with the Leica Qwin v3 software. All the results obtained are shown in the Table 5. As expected the G82B SGI has ferritic-pearlitic matrices while the other cast iron studied has ferritic matrices. In the appendix 4 is shown a figure of the matrix for each cast iron.

Table 5. Graphite and ferrite/pearlite amounts

	Graphite / %	EN Ferrite / %	EN Pearlite / %	ASTM Ferrite / %	ASTM Pearlite / %
G82B SGI 15mm	3.40	35.16	64.84	33.96	62.64
G82B SGI 50mm	7.84	41.89	58.12	38.60	53.56
G82B SGI 75mm	8.80	42.40	57.60	38.67	52.53
G88 SGI 50mm	9.05	100	0	100	0
G89 SGI 15mm	2.12	100	0	100	0
G89 SGI 50mm	6.78	100	0	100	0
G89 SGI 75mm	5.57	100	0	100	0
G88 CGI 50mm	6.09	100	0	100	0
G89 CGI 15mm	2.13	100	0	100	0
G89 CGI 50mm	2.15	100	0	100	0
G89 CGI 75mm	1.94	100	0	100	0

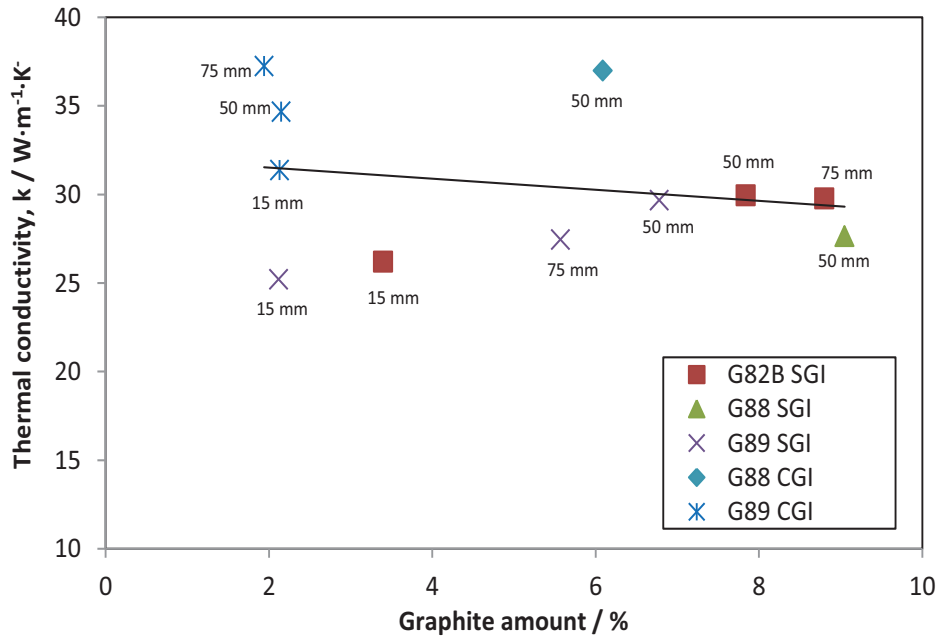


Figure 44. Thermal conductivity versus graphite amount at room temperature

In order to study the thermal conductivity and graphite amount relationship, both properties were plotted in the same graph shown in Figure 44. The fitting line is decreasing with the graphite amount. The expecting result was that the thermal conductivity would raises with the graphite amount due to the high thermal conductivity of graphite. This can be explained because the data of G88 CGI which is very high, if this point would be avoid, the fitting would increases with the graphite amount. In this case the castings with the cooling rate corresponding to a 50 mm thickness don't adjust better to the linear relationship than the casting cooled at the other rates as in nodularity case.

## **5 Discussion and conclusions**

### **5.1 Discussion of method**

#### **5.1.1 Density**

The bulk densities at room temperature of all the casting were measured by Archimedes' method (chapter 3.3). The equipment employed is highly sensible, even a bubble in the distilled water deposit can vary the result, that is why the density was measured twice for each casting, and the average density was obtained. The densities calculated for each casting are between 7.04 and 7.09 g/cm<sup>3</sup>, this density range is close to the density used in other projects working with CGI and SGI [24].

#### **5.1.2 Thermal expansion**

In some others projects as [25] and [26] where the thermal conductivity is studied depending of the temperature, the thermal expansion value is obtained as the slope of the linear regression of the dilatometer heating curve and it is considered constant for all the temperatures range while the cooling curve is not even studied. In order to obtain better thermal expansion value accuracy, in this project both, heating and cooling curves were divided in two ranges, from room temperature to 400 °C, and from 400 to 500 °C. So for each studied material, four thermal expansion values were obtained and are showed in Table 3. With this method the coefficient of determination, denoted as R<sup>2</sup>, raised for all the regression lines where always above 0.99 except for the first studied casting, G82B SGI 15 mm, where R<sup>2</sup> was 0.982.

#### **5.1.3 Specific heat capacity**

The results of the DSC do not give any explication about the behaviour of the silicon content or the cooling ratio, what could cause doubt of the absolute veracity of the c<sub>p</sub> results and because that, the c<sub>p</sub> values used in the thermal conductivity property of each casting can be obtained by the average of all c<sub>p</sub> curves, distinguishing between both, heating and cooling processes. This c<sub>p</sub> values approximation to the average has been carried out in other projects [27] and [28]. In this project the thermal conductivity results obtained from the individual values of c<sub>p</sub> for each material are valid, so the option to work with the averages of c<sub>p</sub> was avoided.

The DSC experiment started the measurements at approximately 40 °C, so the value of  $c_p$  at room temperature is unknown but needed in order to calculate the thermal conductivity at room temperature. The value of  $c_p$  used at room temperature is the equivalent point on the line formed with the 100 and 200 °C corresponding  $c_p$  values for each casting. Generally the line equation is  $y = a \cdot x + b$ . If  $c_{p(100^\circ\text{C})}$  and  $c_{p(200^\circ\text{C})}$  are the  $c_p$  values at 100 and 200 °C respectively, replacing them on the line equation, the  $c_{p(25^\circ\text{C})}$  value at 25 °C can be calculated.

$$\left. \begin{array}{l} c_{p(100^\circ\text{C})} = 100 \cdot a + b \\ c_{p(200^\circ\text{C})} = 200 \cdot a + b \end{array} \right\} \longrightarrow \left\{ \begin{array}{l} a = \frac{c_{p(200^\circ\text{C})} - c_{p(100^\circ\text{C})}}{100} \\ b = 2 \cdot c_{p(100^\circ\text{C})} - c_{p(200^\circ\text{C})} \end{array} \right.$$

Substituting the values of  $a$  and  $b$  in the equation of the line, the  $c_p$  value corresponding to 25 °C is calculated with the expression:

$$c_{p(25^\circ\text{C})} = \frac{c_{p(200^\circ\text{C})} - c_{p(100^\circ\text{C})}}{100} \cdot 25 + 2 \cdot c_{p(100^\circ\text{C})} - c_{p(200^\circ\text{C})} \quad (19)$$

#### 5.1.4 Thermal diffusivity

The results of Laser flash method does not take into account the radiation heat flow, that's why a first correction is applied with the software. The Laser flash method also was performed considering the thermal expansion constant so a second correction is applied to the data obtained with the software. Being the results after the first correction  $\alpha_{D0}$  a second correction is applied and the final data used to calculate the thermal expansion  $\alpha_D$ .

$$\alpha_{D0} = 0.1388 \cdot \frac{L_0^2}{t_{1/2}} \longrightarrow t_{1/2} = 0.1388 \cdot \frac{L_0^2}{\alpha_{D0}}$$

Being  $L_T$  the thickness of the sample at temperature  $T$ , taking into account the elongation due to the temperature increasing. If the equation before is substituted, the diffusivity after correction would be:

$$\alpha_D = 0.1388 \cdot \frac{L_T^2}{t_{1/2}} = 0.1388 \cdot \frac{L_T^2}{0.1388 \cdot \frac{L_0^2}{\alpha_{D0}}} = \alpha_{D0} \cdot \frac{L_T^2}{L_0^2} \quad (20)$$

As explained in the chapter Method and implementation in the dilatometer section (chapter 3.2), the equation of  $L_T$  in the equation below is the line obtained from the dilatometer for each casting and is different between the ranges of temperature from RT to 400 °C and from 400 to 500 °C:

$$\text{From RT to 400 °C: } L_{RT-400^{\circ}\text{C}} = L_0 + L_0 \cdot \alpha_E \cdot (T - T_{RT}) \quad (21)$$

$$\text{From 400 to 500 °C: } L_{400-500^{\circ}\text{C}} = L_{400^{\circ}\text{C}} + L_{400^{\circ}\text{C}} \cdot \alpha_E \cdot (T - T_{400^{\circ}\text{C}}) \quad (22)$$

With this correction the thermal expansion is taking into account for each sample so the results are closer to the reality.

### 5.1.5 Graphite amount

The graphite amount percentage should be inserting in the software to calculate the ferrite and pearlite amount. In order to use the graphite amount values obtained from the nodularity results (in pixels) the microscope live mode resolution ( $A_{total-2}$ ) was calculated using a reference sample with known resolution ( $A_{total-1}$ ) and graphite area ( $A_{graph-1}$ ) in the camera and live mode. The live mode graphite amount of the reference sample was also known ( $A_{graph-2}$ ) from the nodularity results. The percentage of graphite on the reference sample was measured in live and camera mode, both results should be equals:

$$\left. \begin{array}{l} \text{Camera mode: } graph_1(\%) = \frac{A_{graph-1}}{A_{total-1}} \cdot 100 \\ \text{Live mode: } graph_2(\%) = \frac{A_{graph-2}}{A_{total-2}} \cdot 100 \end{array} \right\} \quad (23)$$

Equating the camera and live modes graphite amount equations and solving for the live mode resolution value in pixels is obtained:

$$A_{total-2} = \frac{A_{graph-2}}{A_{graph-1}} \cdot A_{total-1} \quad (25)$$

When the live mode resolution value was obtained the live mode graphite amount percentage ( $graph_2(\%)$ ) was calculated with the equation above.

## **5.2 Discussion of findings**

### **5.2.1 Silicon content and thermal conductivity**

In the present study, no significant influence of silicon content on the thermal conductivity was found. In the case of the SGI, the thermal conductivity values of the castings with different silicon content are in the range 26-32  $\text{W}\cdot\text{m}^{-1}\cdot\text{K}^{-1}$ . In the case of the CGI, the thermal conductivity values of the castings with different silicon content are in the range 30-36  $\text{W}\cdot\text{m}^{-1}\cdot\text{K}^{-1}$ .

### **5.2.2 Cooling rate and thermal conductivity**

In all the castings with cooling rates corresponding to 15 mm of the thickness of plate, the thermal conductivity was lower than the values obtained for the same cast irons with thicker thickness, viz., lower cooling rates. It doesn't occur in the cases of the cooling rates corresponding to 50 and 75 mm thickness. In the case of the SGI, the thermal conductivity values of the castings with different cooling rates are in the range 24-32  $\text{W}\cdot\text{m}^{-1}\cdot\text{K}^{-1}$ . In the case of the CGI, the thermal conductivity values of the castings with different cooling rates are in the range 30-35  $\text{W}\cdot\text{m}^{-1}\cdot\text{K}^{-1}$ .

### **5.2.3 Nodularity and thermal conductivity**

Although there is no significant difference of the thermal conductivity when the silicon content is varied, the thermal conductivity values of CGI are higher than SGI values, and these values become closer when the temperature is increased.

The plots of the thermal conductivity against the nodularity (Figure 42) shows that the castings with cooling rates corresponding to 50 mm shows better linear fitting than the others, that occurs independent of being CGI or SGI.

## **5.3 Conclusions**

- In the present study, no significant influence of silicon content on the thermal conductivity was found. Hence, both CGI and SGI with high silicon content could be employed instead of conventional CGI and SGI in applications without losing required thermal properties if the strength is increased with silicon addition.
- For castings with high cooling ratios (15 mm thickness plate) the thermal conductivity is lower than that of lower cooling rates (50 and 75 mm thicknesses plates). However there is no significant difference between 50 and 75 mm plates. In applications high thermal conductivity is required, hence, it is recommended cooling rates corresponding to thickness thicker than 50 mm from the viewpoint of thermal conductivity.
- Thermal conductivity curve of SGI usually has a maximum point at 200-400 °C. CGI thermal conductivity values of are higher than that of SGI. In some case, the thermal conductivity of CGI has a maximum at 200-300 °C as in SGI.
- In the case of both, CGI and SGI, cooling rates corresponding to 50 mm shows better fitting than the others rates when plotting the thermal conductivity against the nodularity.

## **6 Future work**

- The influence of matrices (ferritic, pearlitic and/or cementite) on the thermal conductivity.
- The influence of wide range of silicon amount on the thermal conductivity.
- The influence of other components such as Mn, P or S on the thermal conductivity.
- The influence of cooling rate should be discussed quantitatively.

## **7 Acknowledgements**

The author would like to thank the following people:

- My supervisors Lennart Elmquist and Taishi Matsushita for great supervision and advices.
- Lars Johansson for his technical skills in the workshop.
- Toni Bogdanoff for his technical skills in the laboratory.
- Ari Badal and Juan Carlos Hernando for joy inside and outside the university.
- Alvaro Solana, Patricia Sánchez and Sonia Baroudi for all this year.
- My family, because with them I learn a new thing every day.

## 8 References

- [1] Holmgren, D., Diószegi, A. and Svensson, I. L. *Parameters Influencing the Temperature Distribution in Cast Iron Cylinder Heads Operating at Elevated Temperatures*. Paper presented at the 8<sup>th</sup> international symposium on science & processing of cast iron, SPCI8, Beijing, China, (2006).
- [2] <http://en.wikipedia.org/wiki/iron> (Acc. 2 February 2013)
- [3] Spoerl, J. S., A brief history of iron and steel production, Saint Anselm University, USA. <http://www.anselm.edu/homepage/dbanach/h-camegie-steel.htm> (Acc. 30 November 2012)
- [4] Yeng, T. H. and Eng, T. H. The ferrous data metals book. Chapter 1. [http://www.oocities.org/ferritec\\_eng](http://www.oocities.org/ferritec_eng) (Acc. 15 November 2012)
- [5] Bramfitt, B. L., Benschoter A. O., *Metallographer's guide: practices and procedures for irons and steels*, ASM International, USA, (2002).
- [6] Pollack, H. W., *Materials science and metallurgy* (4<sup>th</sup> edition), Prentice Hall USA, (1988).
- [7] Rack, P. D., A review of Callister, Iron-Carbon Phase Diagram, University of Tennessee, USA. <http://web.utk.edu/~prack/MSE%20300/FeC.pdf> (Acc. 30 November 2012)
- [8] Stefanescu D. M., *Solidification and modelling of cast iron - A short history of the defining moments*, The Ohio State University, USA. Published in *Materials Science and Engineering A* 413–414 (2005) pp. 322–333.
- [9] Department of the Navy, Bureau of Ships: *Foundry manual*, Washington D.C., USA, (1958).
- [10] Berglund, P. L., <http://threeplanes.net/cementite.html> (Acc. 25 May 2013)

- [11] König, M., *Literature Review of Microstructure Formation in Compacted Graphite Iron*, International Journal of Cast Metals Research (2010) Vol. 3 (3), pp. 185-192.
- [12] Holmgren, D., *Review of the thermal conductivity of cast iron*, International Journal of Cast Metals Research (2005) Vol. 23 (18), pp. 331-345.
- [13] Nano Enhanced Wholesale Newtechs (2008) <http://www.nano-enhanced-wholesale-technologies.com/faq/carbon-forms.htm> (Acc. 25 May 2013)
- [14] Setién, J. and Varona, J. M. *Apuntes de fundamentos de ciencia y tecnología de materiales*, University of Cantabria, Spain, (2003).
- [15] Key to metals database <http://www.keytometals.com> (Acc. 30 November 2012)
- [16] Elmquist, L. *Defect Formation during Solidification in Grey Iron Castings*, PhD thesis, Chalmers University of Technology, Gothenburg, Sweden, (2009).
- [17] König, M. *Microstructure formation during solidification and solid state transformation in compacted graphite iron*, PhD thesis, Chalmers University of Technology, Gothenburg, Sweden, (2011).
- [18] Voort, G. V., 75 Years of Metallography, the ASTM Committee E-4 Perspective, ASTM Standardization News, USA, (1991).
- [19] Netzsch Group <http://www.netzsch-thermal-analysis.com> (Acc. 30 November 2012)
- [20] Parker, W. J., Jenkins, R. J., Butler, C. P. and Abbott, G. L., *Flash method of determining thermal diffusivity, heat capacity and thermal conductivity*, Journal of applied Physics (1961) 32, pp. 1679.
- [21] Struers <http://www.struers.com> (Acc. 26 May 2013)
- [22] Davis, J. R. *ASM Specialty Handbook: Cast irons*, ASM International, USA, (1996).

- [23] Holmgren, D., Diószegi, A. and Svensson, I. L., *Effects of nodularity on the thermal conductivity of cast iron*, International Journal of Cast Metals Research (2007), Vol. 20, pp. 30-40(11).
- [24] Holmgren, D., *Thermal conductivity of Cast Iron*, PhD thesis, Chalmers University of Technology, Gothenburg, Sweden, (2006).
- [25] Selin, M., *On thermal conductivity and strength of compacted graphite iron*, PhD thesis, Chalmers University of Technology, Gothenburg, Sweden, (2010).
- [26] Holmgren, D., Källbom, R. and Svensson, I. L. *Influences of the graphite growth direction on the thermal conductivity of cast iron*, Metallurgical and Material Transactions A (2007), Vol. 38, pp. 268-75.
- [27] Selin, M., *Tensile and thermal properties in compacted graphite irons at elevated temperatures*, Metallurgical and Materials Transactions A (2010), Vol. 41, pp. 3100-3109.
- [28] Holmgren, D., Diószegi, A. and Svensson, I. L., *Effects of carbon content and solidification rate on the thermal conductivity of grey cast iron*. Proceedings of the 8<sup>th</sup> international symposium on science & processing of cast iron, SPCI8, (2006), Beijing, China.

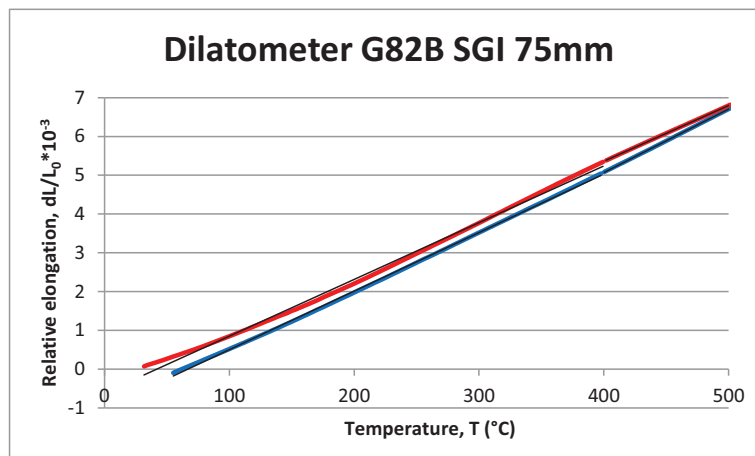
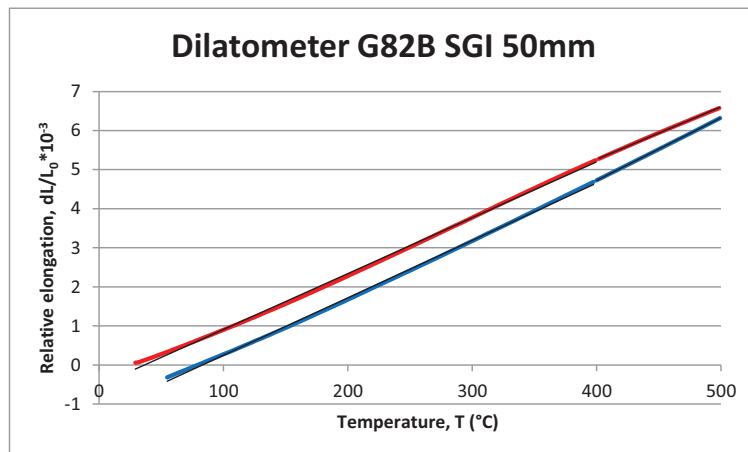
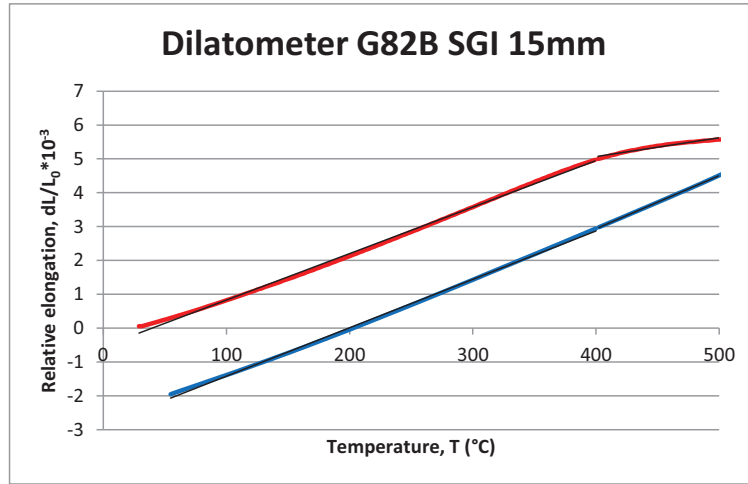
## 9 Appendices

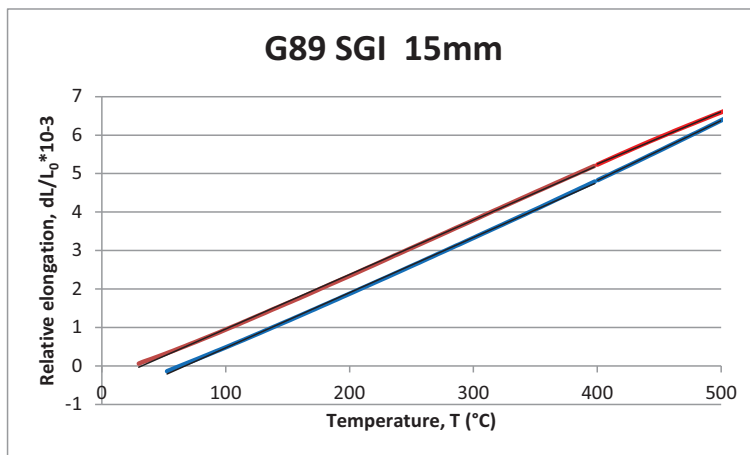
Appendix 1. Complete analysis of the components of each cast iron.

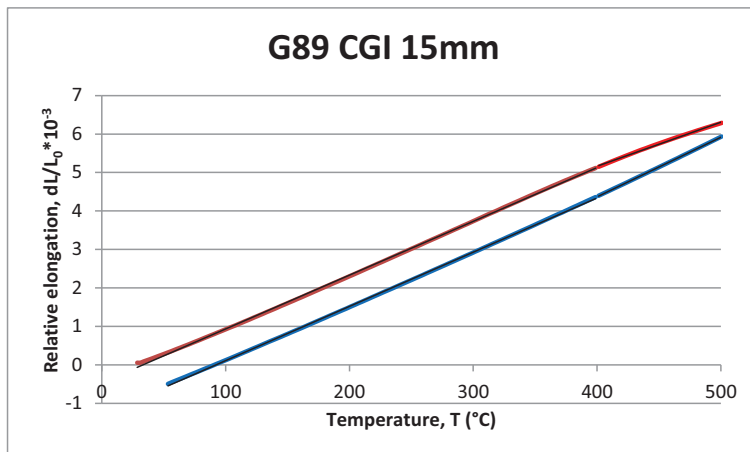
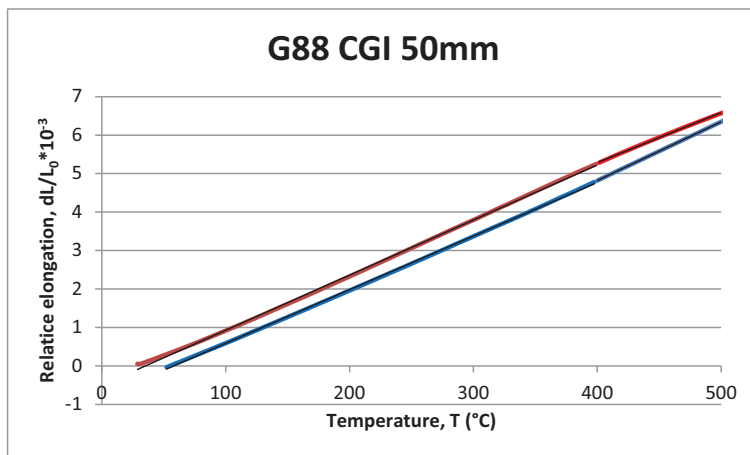
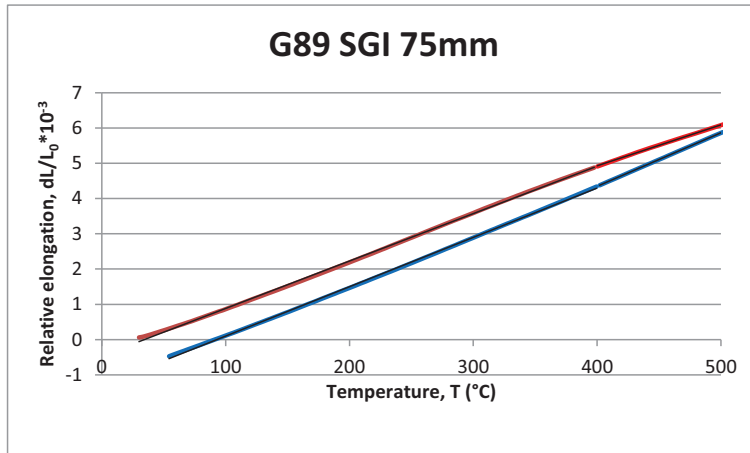
Table 6. Complete components analysis of each casting

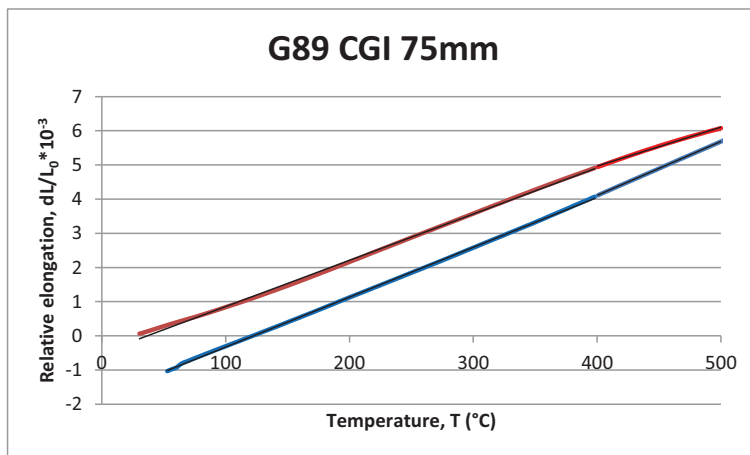
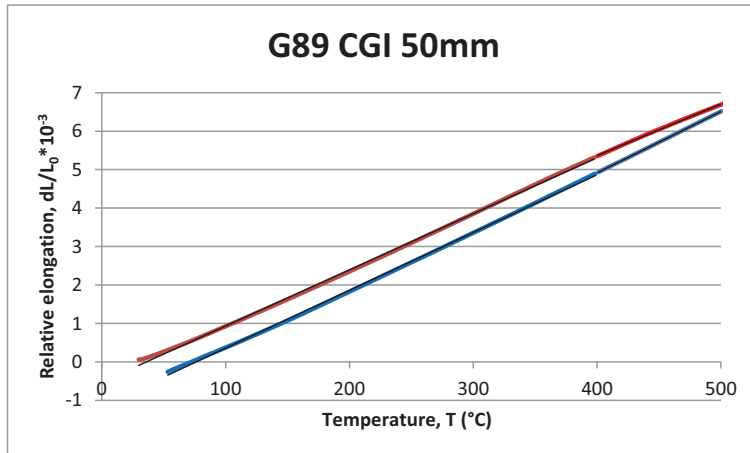
Element	G82B SGI	G88 SGI	G89 SGI	G88 CGI	G89 CGI
<b>C</b>	3.51	3.28	3.13	3.24	3.18
<b>Si</b>	2.36	3.73	4.25	3.44	3.87
<b>Mn</b>	0.408	0.169	0.169	0.17	0.167
<b>P</b>	0.0063	0.009	0.0095	0.0069	0.0072
<b>S</b>	0.0043	0.0056	0.0065	0.0062	0.0072
<b>Cr</b>	0.025	0.028	0.029	0.028	0.028
<b>Ni</b>	0.039	0.045	0.041	0.048	0.047
<b>Mo</b>	0.0028	0.0012	0.0016	0.0034	0.0037
<b>Al</b>	0.0083	0.0085	0.01	0.0045	0.0057
<b>Cu</b>	0.294	0.039	0.036	0.035	0.034
<b>Co</b>	0.024	0.03	0.03	0.032	0.032
<b>Ti</b>	0.0059	0.011	0.012	0.011	0.011
<b>Nb</b>	0.001	0.001	0.001	-	-
<b>V</b>	0.0057	0.012	0.012	0.011	0.011
<b>W</b>	0.007	0.007	0.007	-	-
<b>Pb</b>	0.001	0.001	0.001	<0.0010	<0.0010
<b>Mg</b>	0.036	0.037	0.036	0.0061	0.0062
<b>B</b>	0.0058	0.0053	0.0053	0.0057	0.0073
<b>Sb</b>	0.0038	0.0062	0.0053	0.014	0.014
<b>Sn</b>	0.0028	0.0029	0.003	0.0028	0.0029
<b>Zn</b>	0.001	0.001	0.001	<0.0010	<0.0010
<b>As</b>	0.0033	0.0033	0.0033	0.0026	0.0017
<b>Bi</b>	0.0015	0.0015	0.0015	<0.0015	<0.0015
<b>Ce</b>	0.0022	0.002	0.002	0.008	0.0069
<b>Zr</b>	0.0023	0.0015	0.0015	<0.0015	0.0017
<b>La</b>	0.0014	0.0005	0.0005	-	-
<b>Se</b>	0.055	0.059	0.056	0.0055	0.0041
<b>N</b>	0.0064	0.003	0.0027	0.0091	0.0068
<b>Fe</b>	93.2	92.5	92.1	-	-
<b>CE</b>	4.30	4.53	4.55	4.39	4.47

Appendix 2. Regression lines calculated with Excel of curves given for the dilatometer, relative elongation variation of the sample with the temperature for both, heating (red curves) and cooling processes (blue curves).









Appendix 3. Sources tables of all thermal conductivity graphics.

Table 7. Thermal conductivity values of casting G82B SGI 15 mm

T / °C	$\rho_{RT} / \text{g}\cdot\text{cm}^{-3}$	$\alpha_E / \text{K}^{-1}$	$\rho_{RT} / \text{g}\cdot\text{cm}^{-3}$	$c_p / \text{J}\cdot\text{g}^{-1}\cdot\text{K}^{-1}$	$\alpha_D / \text{mm}^2\cdot\text{s}\cdot\text{g}^{-1}$	$k / \text{W}\cdot\text{m}^{-1}\cdot\text{K}^{-1}$
<b>25</b>	7.0755	14.4591	7.0755	0.46	10.27	33.68
<b>100</b>	7.0755	14.4591	7.0526	0.49	9.95	34.03
<b>200</b>	7.0755	14.4591	7.0222	0.51	9.66	34.85
<b>300</b>	7.0755	14.4591	6.9921	0.55	9.01	34.58
<b>400</b>	7.0755	14.4591	6.9622	0.59	8.27	34.10
<b>500</b>	7.0755	13.4258	7.0471	0.63	7.38	32.65

Table 8. Thermal conductivity values of casting G82B SGI 50 mm

T / °C	$\rho_{RT} / \text{g}\cdot\text{cm}^{-3}$	$\alpha_E / \text{K}^{-1}$	$\rho_{RT} / \text{g}\cdot\text{cm}^{-3}$	$c_p / \text{J}\cdot\text{g}^{-1}\cdot\text{K}^{-1}$	$\alpha_D / \text{mm}^2\cdot\text{sg}^{-1}$	$k / \text{W}\cdot\text{m}^{-1}\cdot\text{K}^{-1}$
25	7.0538	14.099	7.0538	0.48	10.57	35.64
100	7.0538	14.099	7.0315	0.49	10.28	35.46
200	7.0538	14.099	7.0020	0.51	9.85	34.98
300	7.0538	14.099	6.9727	0.53	9.18	33.97
400	7.0538	14.099	6.9437	0.56	8.47	33.06
500	7.0538	13.0755	7.0262	0.59	7.55	31.41

Table 9. Thermal conductivity values of casting G82B SGI 75 mm

T / °C	$\rho_{RT} / \text{g}\cdot\text{cm}^{-3}$	$\alpha_E / \text{K}^{-1}$	$\rho_{RT} / \text{g}\cdot\text{cm}^{-3}$	$c_p / \text{J}\cdot\text{g}^{-1}\cdot\text{K}^{-1}$	$\alpha_D / \text{mm}^2\cdot\text{sg}^{-1}$	$k / \text{W}\cdot\text{m}^{-1}\cdot\text{K}^{-1}$
25	7.0379	13.2007	7.0379	0.49	10.31	35.28
100	7.0379	13.2007	7.0171	0.50	9.96	35.14
200	7.0379	13.2007	6.9895	0.52	9.50	34.86
300	7.0379	13.2007	6.9621	0.56	8.94	34.98
400	7.0379	13.2007	6.9349	0.60	8.30	34.40
500	7.0379	11.4105	7.0139	0.63	7.39	32.76

Table 10. Thermal conductivity values of casting G89 SGI 15 mm

T / °C	$\rho_{RT} / \text{g}\cdot\text{cm}^{-3}$	$\alpha_E / \text{K}^{-1}$	$\rho_{RT} / \text{g}\cdot\text{cm}^{-3}$	$c_p / \text{J}\cdot\text{g}^{-1}\cdot\text{K}^{-1}$	$\alpha_D / \text{mm}^2\cdot\text{sg}^{-1}$	$k / \text{W}\cdot\text{m}^{-1}\cdot\text{K}^{-1}$
25	7.0655	13.9586	7.0655	0.47	7.46	24.70
100	7.0655	13.9586	7.0434	0.48	7.51	25.31
200	7.0655	13.9586	7.0141	0.49	7.54	26.00
300	7.0655	13.9586	6.9851	0.50	7.30	25.46
400	7.0655	13.9586	6.9563	0.52	6.88	24.91
500	7.0655	13.6048	7.0368	0.56	6.26	24.50

Table 11. Thermal conductivity values of casting G89 SGI 50 mm

T / °C	$\rho_{RT} / \text{g}\cdot\text{cm}^{-3}$	$\alpha_E / \text{K}^{-1}$	$\rho_{RT} / \text{g}\cdot\text{cm}^{-3}$	$c_p / \text{J}\cdot\text{g}^{-1}\cdot\text{K}^{-1}$	$\alpha_D / \text{mm}^2\cdot\text{sg}^{-1}$	$k / \text{W}\cdot\text{m}^{-1}\cdot\text{K}^{-1}$
25	7.0861	14.0423	7.0861	0.48	8.11	27.37
100	7.0861	14.0423	7.0638	0.50	8.23	29.06
200	7.0861	14.0423	7.0342	0.53	8.16	30.52
300	7.0861	14.0423	7.0049	0.56	7.90	31.09
400	7.0861	14.0423	6.9759	0.60	7.39	31.17
500	7.0861	10.7024	7.0634	0.66	6.69	31.22

Table 12. Thermal conductivity values of casting G89 SGI 75 mm

T / °C	$\rho_{RT} / \text{g}\cdot\text{cm}^{-3}$	$\alpha_E / \text{K}^{-1}$	$\rho_{RT} / \text{g}\cdot\text{cm}^{-3}$	$c_p / \text{J}\cdot\text{g}^{-1}\cdot\text{K}^{-1}$	$\alpha_D / \text{mm}^2\cdot\text{sg}^{-1}$	$k / \text{W}\cdot\text{m}^{-1}\cdot\text{K}^{-1}$
25	7.0704	13.1204	7.0704	0.46	8.07	26.11
100	7.0704	13.1204	7.0496	0.47	8.01	26.66
200	7.0704	13.1204	7.0220	0.49	8.01	27.64
300	7.0704	13.1204	6.9947	0.52	7.68	27.69
400	7.0704	13.1204	6.9676	0.54	7.15	26.70
500	7.0704	11.7406	7.0456	0.57	6.47	26.02

Table 13. Thermal conductivity values of casting G88 SGI 50 mm

T / °C	$\rho_{RT} / \text{g}\cdot\text{cm}^{-3}$	$\alpha_E / \text{K}^{-1}$	$\rho_{RT} / \text{g}\cdot\text{cm}^{-3}$	$c_p / \text{J}\cdot\text{g}^{-1}\cdot\text{K}^{-1}$	$\alpha_D / \text{mm}^2\cdot\text{sg}^{-1}$	$k / \text{W}\cdot\text{m}^{-1}\cdot\text{K}^{-1}$
25	7.0504	13.3837	7.0504	0.48	7.90	26.64
100	7.0504	13.3837	7.0292	0.49	8.09	27.90
200	7.0504	13.3837	7.0012	0.51	8.09	28.73
300	7.0504	13.3837	6.9734	0.53	7.79	28.82
400	7.0504	13.3837	6.9458	0.56	7.29	28.46
500	7.0504	7.3606	7.0349	0.59	6.56	27.33

Table 14. Thermal conductivity values of casting G89 CGI 15 mm

T / °C	$\rho_{RT} / \text{g}\cdot\text{cm}^{-3}$	$\alpha_E / \text{K}^{-1}$	$\rho_{RT} / \text{g}\cdot\text{cm}^{-3}$	$c_p / \text{J}\cdot\text{g}^{-1}\cdot\text{K}^{-1}$	$\alpha_D / \text{mm}^2\cdot\text{sg}^{-1}$	$k / \text{W}\cdot\text{m}^{-1}\cdot\text{K}^{-1}$
25	7.0755	13.7515	7.0755	0.47	9.40	30.98
100	7.0755	13.7515	7.0537	0.48	9.36	31.71
200	7.0755	13.7515	7.0248	0.50	9.06	31.78
300	7.0755	13.7515	6.9961	0.53	8.58	32.04
400	7.0755	13.7515	6.9677	0.57	7.98	31.46
500	7.0755	11.5045	7.0512	0.60	7.17	30.46

Table 15. Thermal conductivity values of casting G89 CGI 50 mm

T / °C	$\rho_{RT} / \text{g}\cdot\text{cm}^{-3}$	$\alpha_E / \text{K}^{-1}$	$\rho_{RT} / \text{g}\cdot\text{cm}^{-3}$	$c_p / \text{J}\cdot\text{g}^{-1}\cdot\text{K}^{-1}$	$\alpha_D / \text{mm}^2\cdot\text{sg}^{-1}$	$k / \text{W}\cdot\text{m}^{-1}\cdot\text{K}^{-1}$
25	7.0755	14.4591	7.0755	0.46	10.27	33.68
100	7.0755	14.4591	7.0526	0.49	9.95	34.03
200	7.0755	14.4591	7.0222	0.51	9.66	34.85
300	7.0755	14.4591	6.9921	0.55	9.01	34.58
400	7.0755	14.4591	6.9622	0.59	8.27	34.10
500	7.0755	13.4258	7.0471	0.63	7.38	32.65

Table 16. Thermal conductivity values of casting G89 CGI 75 mm

T / °C	$\rho_{RT} / \text{g}\cdot\text{cm}^{-3}$	$\alpha_E / \text{K}^{-1}$	$\rho_{RT} / \text{g}\cdot\text{cm}^{-3}$	$c_p / \text{J}\cdot\text{g}^{-1}\cdot\text{K}^{-1}$	$\alpha_D / \text{mm}^2\cdot\text{sg}^{-1}$	$k / \text{W}\cdot\text{m}^{-1}\cdot\text{K}^{-1}$
25	7.0379	13.2007	7.0379	0.49	10.31	35.28
100	7.0379	13.2007	7.0171	0.50	9.96	35.14
200	7.0379	13.2007	6.9895	0.52	9.50	34.86
300	7.0379	13.2007	6.9621	0.56	8.94	34.98
400	7.0379	13.2007	6.9349	0.60	8.30	34.40
500	7.0379	11.4105	7.0139	0.63	7.39	32.76

Table 17. Thermal conductivity values of casting G88 CGI 50 mm

T / °C	$\rho_{RT} / \text{g}\cdot\text{cm}^{-3}$	$\alpha_E / \text{K}^{-1}$	$\rho_{RT} / \text{g}\cdot\text{cm}^{-3}$	$c_p / \text{J}\cdot\text{g}^{-1}\cdot\text{K}^{-1}$	$\alpha_D / \text{mm}^2\cdot\text{sg}^{-1}$	$k / \text{W}\cdot\text{m}^{-1}\cdot\text{K}^{-1}$
25	7.0538	14.099	7.0538	0.48	10.57	35.64
100	7.0538	14.099	7.0315	0.49	10.28	35.46
200	7.0538	14.099	7.0020	0.51	9.85	34.98
300	7.0538	14.099	6.9727	0.53	9.18	33.97
400	7.0538	14.099	6.9437	0.56	8.47	33.06
500	7.0538	13.0755	7.0262	0.59	7.55	31.41

Appendix 4. Pictures taken with the microscope of each studied cast iron. The left figure shows the graphite and the right figure the matrix.

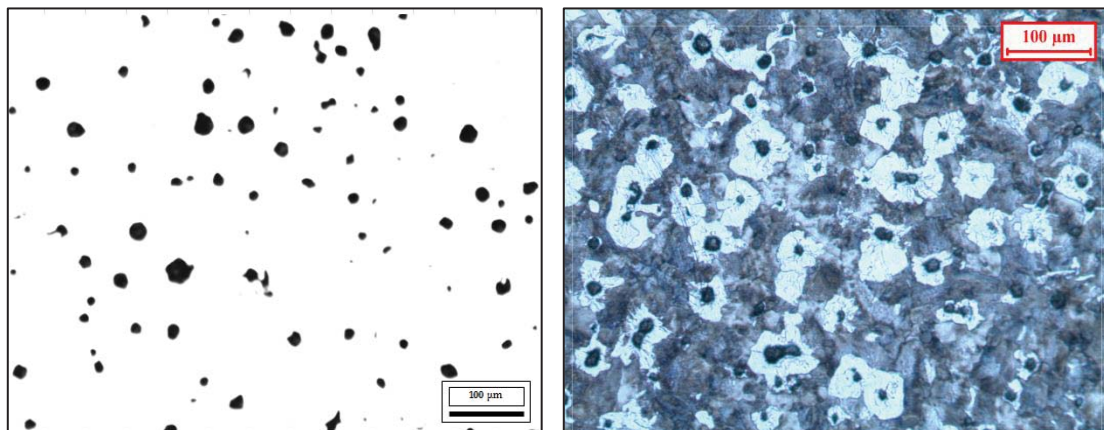


Figure 45. G82B SGI 15 mm

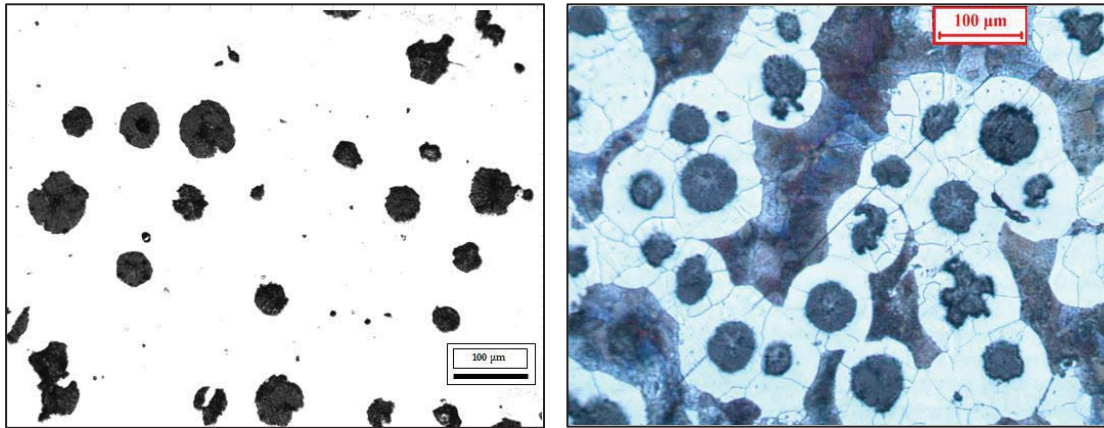


Figure 46. G82B SGI 50 mm

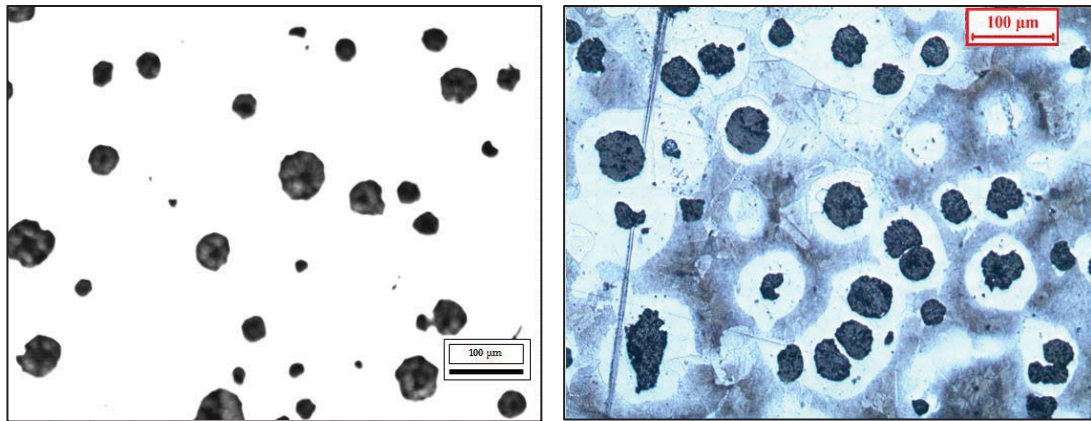


Figure 47. G82B SGI 75 mm

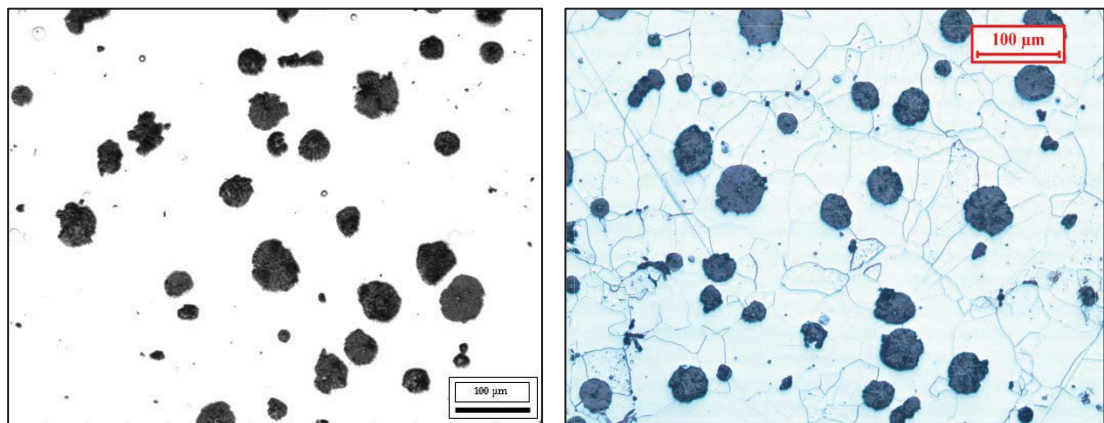


Figure 48. G88 SGI 50 mm

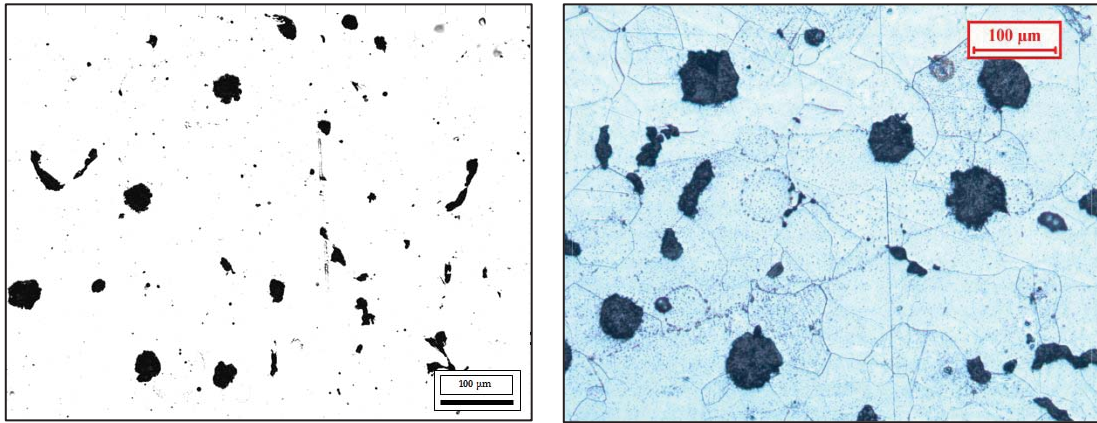


Figure 49. G89 SGI 15 mm

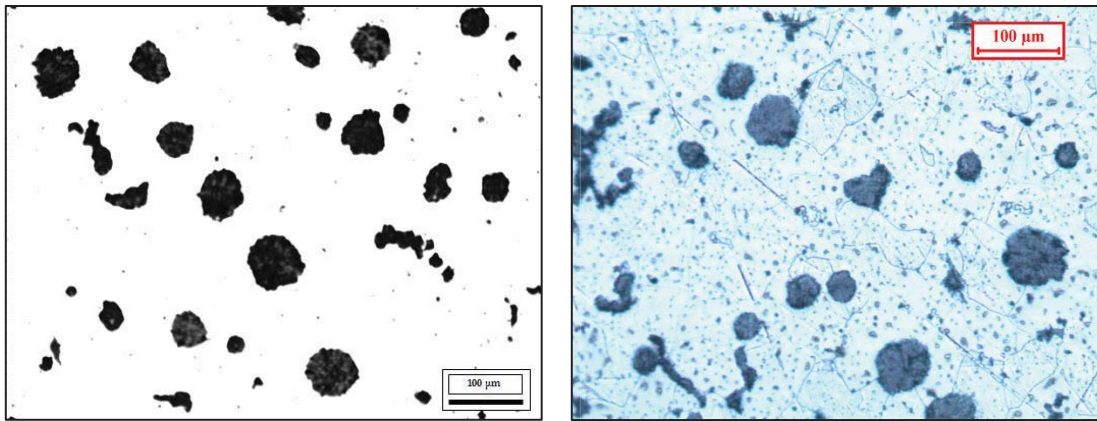


Figure 50. G89 SGI 50 mm

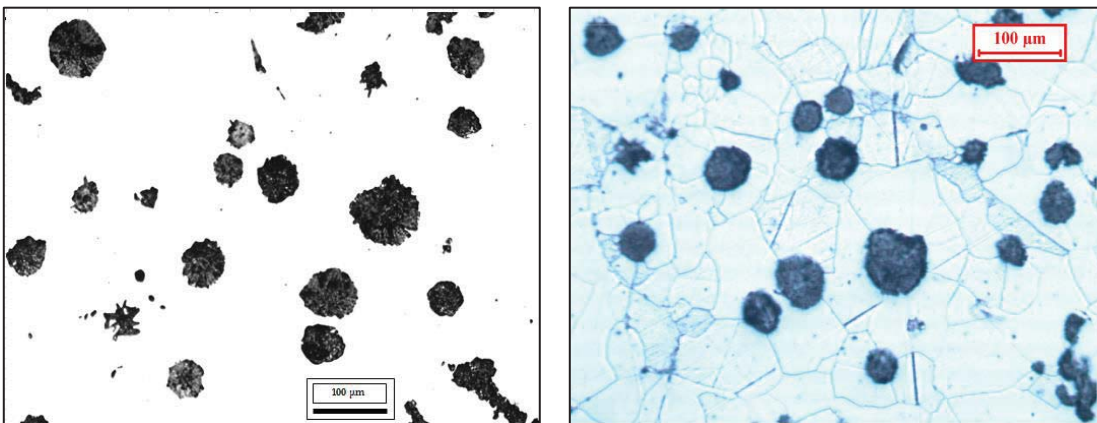


Figure 51. G89 SGI 75 mm

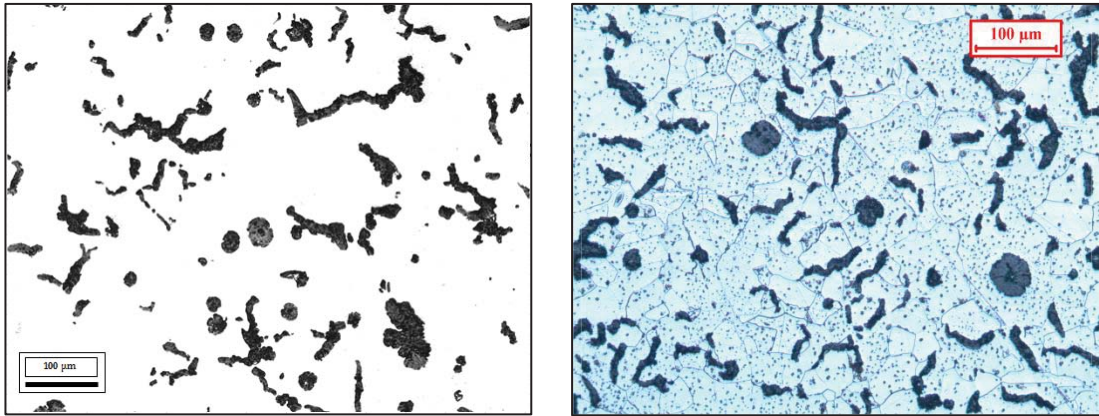


Figure 52. G88 CGI 50 mm

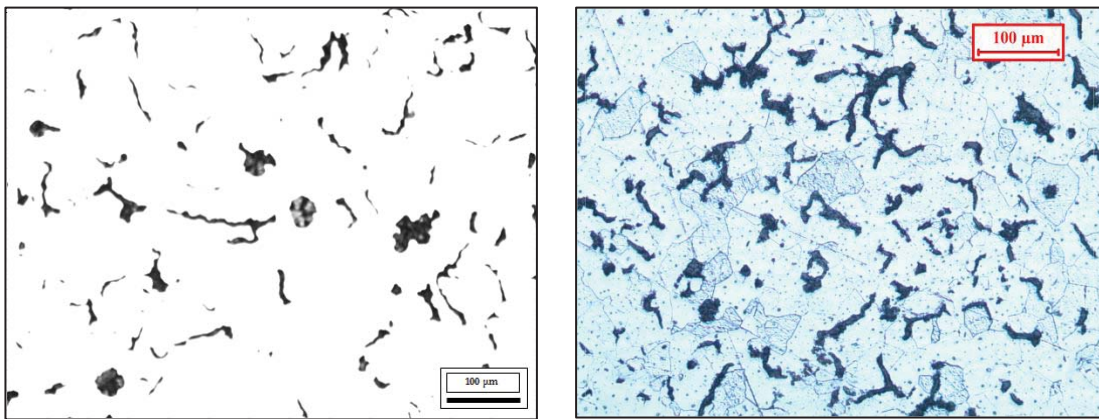


Figure 53. G89 CGI 15 mm

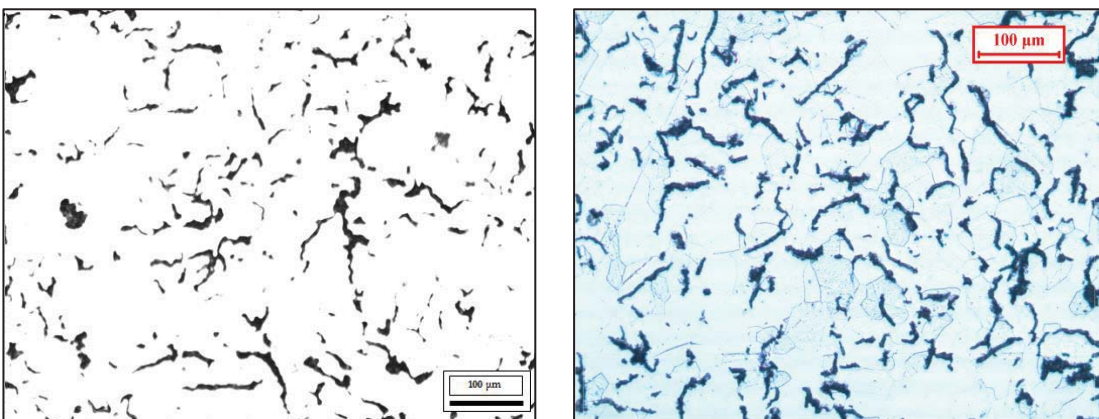


Figure 54. G89 CGI 50 mm

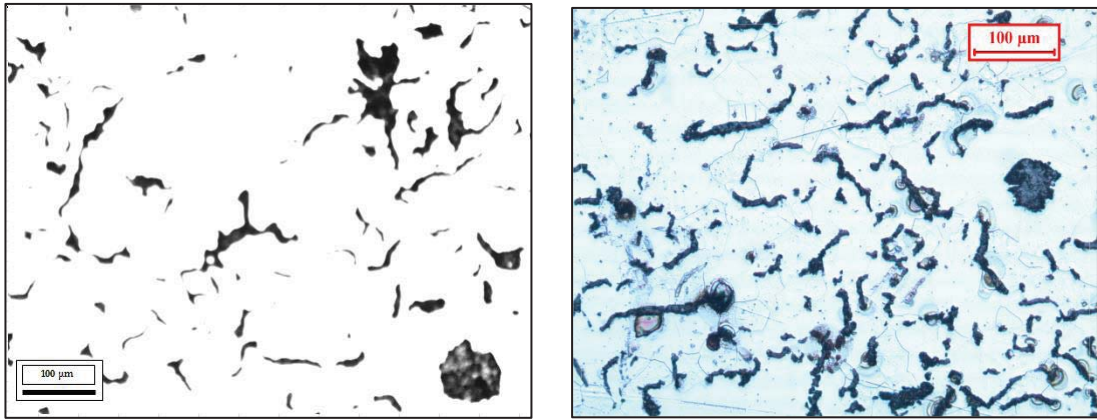


Figure 55. G89 CGI 75 mm